CHAPTER 3

MEASUREMENTS OF TOTAL SCATTERING CROSS SECTION.

3.1. Introduction.

Photons interact in a number of ways with atomic electrons, nuclei or fields of nuclei and of electrons. In low γ -ray energy range, the most important interactions are: (1) incoherent scattering by atomic electrons (2) coherent Rayleigh scattering by atomic electrons (3) photoelectric absorption by atoms and (4) electron positron pair production in the field of the nucleus. The remaining interaction processes produce negligible effects in the low energy region. These are the resonance scattering and Thomson scattering by the nucleus, Delbrück scattering by the electric field of the nucleus, two photon Compton scattering and the photonuclear interactions etc. and will be omitted in the present discussion. Consequently, the total photon interaction cross section per atom is given by the sum of the cross sections for the fundamental processes (1) to (4). This cross section depends on the photon energy and the atomic number Z of the atom.

A narrowly collimated beam of monoenergetic gamma ray photons shows truly exponential attenuation in matter under some experimental conditions. An exponential attenuation is due to the fact that photons are attenuated in the first collisions. As a result, a measurement of transmission of a narrowly collimated beam of photons through a slab of absorber of known thickness by a narrowly collimated detector enables the determination of the total cross section.

The experimental conditions to impose are the following:

(a) All photons which are singly scattered in the absorber even at very small angles and all other secondary photons produced in the absorber must not be detected. That is, only those collimated primary photons which penetrate the absorber without interaction sould be detected. The geometry of an experimental setup under this condition is known as good gemmetry.

(b) The multiply scattered photons in the absorber must not affect the good geometry condition of the primary beam after transmission. That is, the multiply scattered photons must not be detected along with the transmitted primary photons.

The second condition has not been preserved in many of the previous transmission measurements (Table 3.1). Inconsistency of the published experimental results by the different authors for the same elements at the same energies and discrepancies between some of the experimental results and the theoretical estimates available at their measurements have also been noticed (Co 70, Ph 68).

All these facts point to the necessity of new measurements of total photon cross sections of elements which have previously been measured and further measurements on additional elements which have not been covered in the earlier measurements. This necessity is more urgent because of recent developments in the theories of different photon interaction processes (Cr 67, 68, Ve 71, Sc 73, Øv 68, 70). Quantitative comparison of the experimental data with the presently available refined theories is as important as the development of the theories themselves. This has been the strongest point for the present set of measurements of total photon cross sections.

TABLE 3.1

Summary of published work from 1920 to 1973 in the photon energy region 600 - 1400 KeV for elements chosen in the present work. (ION-Ion-Chamber, GM-GM counter, SC-Scintillation counter, SD-Semiconductor detector).

Element	Z	Reference (Detector used, number of energies when specified).
Hydrogen	1	No published data
Lithium	3	No published data
Boron	5	No published data
Carbon	6	C48(GM,5), Co52(SC,6), Wy52(GM,6), Sh52(GM,1), Ma57(SC,4), La61(SC,6), Ba62(SC,4), Mu64(SC,6), Co70(SC,9), He71(SD)
Nitrogen	7	No published data
Oxygen	8	Gh53(GM,1)
Fluorine	9	No published data
Sodium	11	Qu66(SC,4)
Magnesium	12	Sh52(G M,1), C70(SC,9)
Aluminium	13	Ma47(Ion,1), Al48(GM,2), Pa49(GM,2), Da51(GM,4), Sh52(GM,1), Wy52(GM,4), Co52(SC,2), Gh53(GM,1) Ma57(SC), Bo58(GM,1), La61(SC,4), Ba62(SC), Ra63(SC,6), Ma64(SC,6), Ka67(SC,1), Ma70(SC,3), Co70(SC,9), He71(SD)
Silicon	14	Ma70(SC,3), Ba58(GM,1)
Sulfur	16	Sh52(GM,1), Co70(SC,9)
Potassium	19	No published data

TABLE 3.1(Contd.)

Element	Z	Reference (Detector used, number of energies when specified).
Calcium	20	Sh52(GM,1)
Titanium	22	Sh52(GM,1), Co70(SC,9), He71(SD)
Iron	26	C45(GM,2), Ma47(Ion), Sh52(GM,1), Ba62(SC) Ka67(SC), Ma70(SC,3), Co70(SC,9)
Zinc	30	Sh52(GM,1), Gh57(SC,1), Bo58(GM,1), Co70(SC,9)
Germanium	32	Bo58(GM,1)
Arsenic	33	No published data
Bromine	35	Gh53,57(GM,SC,1)
Rubidium	37	No published data.
Molybdenum	42	Sh52(GM,1), Wy52(GM,4), Co70(SC,9), He71(SD)
Iodine	53	Ho54(SC,3), Gh53(GM,1)
Cesium	55	No published data
Lanthanum	57	Co70(SC,9)
Cerium	58	No published data
Neodymium	60	No published data
Samarium	62	No published data
Gadolinium	64	Co70(SC,9)
Dysprosium	66	No published data
Ytterbium	70	No published data
Mercury	80	Sh52(GM,1), Gh57(SC,1), Mu64(SC,4), Qu66(SC,5)

TABLE 3.1(Contd.)

Element	Z	Reference (Detector used, number of photon energies when specified).
Lead	82	Co45(GM,2), Ma47(Ion,1), Al48(GM,2), Co48(GM,2), Da51(GM,4), Sh52(GM,1), Wy52(GM,4), Co52(SC,2), Gh53(GM,1), Ma57(SC), Gh57(SC,1), Bo58(GM,1), La61(SC,4), Ka60(SC,2), Ba62(SC),Ma63(SC,6), Ka67(SC,1),We69(SC,1),Ma70(SC,3), Co70(SC,9), He71(SD), Ra73(SC,12).

3.2. Experimental arrangements.

The principle of transmission method under ideal conditions is quite simple and straightforward. Deviations from the ideal good geometry conditions lead to uncertainty in the measurements. The multiple scattering in the absorber thickness can also introduce error in the measurements.

3.2.1. Collimation of gamma ray source and the detector.

The experimental setup (Fig.3.1, Table 3.2) has been arranged under rigorous collimation requirements to obtain good geometry condition for the primary beam before and after transmission and to reduce the background photons from the materials other than the absorber slab.

The gamma ray source was within a 10 cm deep conical bore in a lead block. The minimum thickness of lead shielding at the side and the back of the source was 20 cm. The collimator No.1 is a 23 cm thick iron block having a collimating bore of exit aperture 0.4 cm. The collimation of the primary beam between the absorber and the detector was provided by colli-

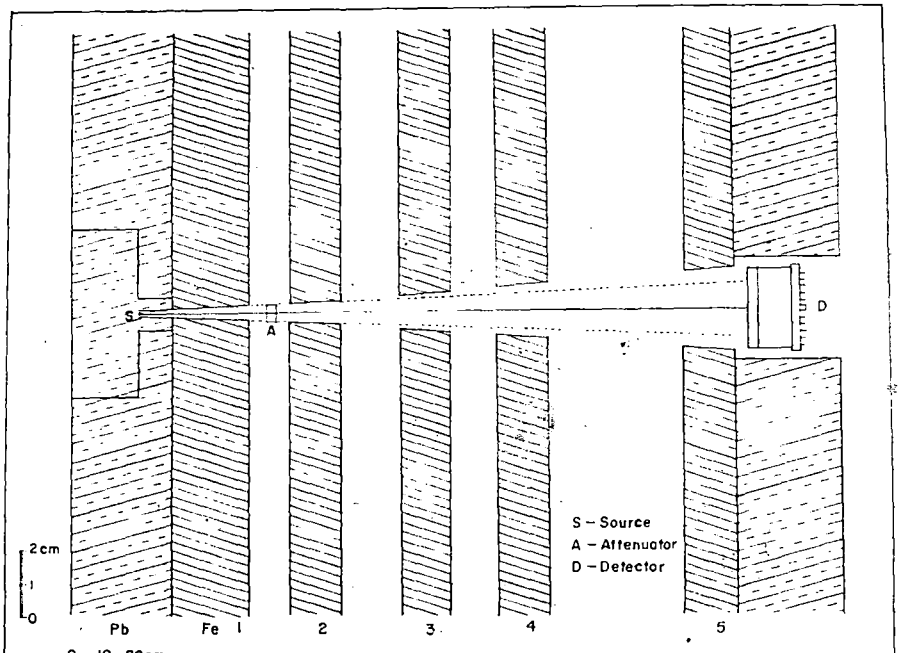

Fig.3.1.Schematic diagram of the experimental arrangement.

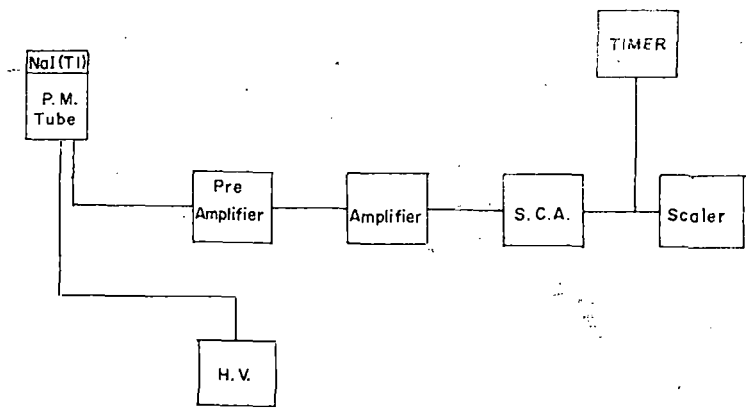

Fig-3.2 SCA SYSTEM SET-UP

mators Nos. 2 - 5 of total thickness 60 cm of iron. The collimator shields prevent photons scattered in the shields and in the environs from reaching the detector. The collimators were mounted on a rigid optical bench of iron so that these could be adjusted in position to obtain different geometry factors and to study the effect of geometry factors on the measurements.

TABLE 3.2

Basic data for the narrow beam geometry(Fig.3.1).

1. Source-to-detector distance 175 cm.
2. Source diameter 0.3 cm.
3. Detector diameter 2.4 cm.
4. Absorber diameter 0.5 cm.

Absorber-to-detector distance (cm)	Maximum scattering angle θ_o, for scattered photons	Maximum solid angle(sr) of the scattering cone from absorber to detector centre
135	27'	10.7×10^{-6}
120	23'	13.3×10^{-6}
100	20'	19.5×10^{-6}
75	20'	24.85×10^{-6}

3.2.2. Precaution against small angle single scattering.

As already stated, the detector should respond only to primary photons which pass through the absorber without experiencing any interaction. Photons which are incoherently or coherently scattered at small angles can not be resolved out from the primary photons which have had no interaction. At small angle, the coherent Rayleigh scattering cross section and the incoherent scattering

cross section vary rapidly. The effect can be minimised to a negligible extent if the solid angle of the collimating system between the absorber and the detector is made very small.

In the geometry of the present setup, no photon scattered in the absorber at an angle greater than 27' could reach the detector. Even in this setup the effect has been investigated by making measurements at three different solid angles obtained by changing the positions of the collimators and the absorber.

3.2.3. Precaution against Multiple scattering.

If the thickness of the absorber is not suitably chosen, a significant number of multiply scattered photons from the absorber may reach the detector. It is possible to minimise the effect by narrowly collimating the transmitted beam of photons and by measuring transmission through small absorber thickness. In the course of the present measurements the effect has been investigated. Some measured spectral shapes without the absorber and with different absorber thicknesses have been included together with the corresponding values of attenuation coefficients. It is found that the effect is negligible for absorber thickness within two mean-free-path(mfp = $\frac{1}{\mu}$) of primary photons. For measurement with each absorber, the maximum thickness to be used was determined in trial experimental runs under the requirement that the full width at half maximum of the full energy peak (photo peak) of the primary photon spectrum is not changed when the absorber is put in the beam.

3.2.4. Requirements in the detector system.

Even with the high degree of collimation of the photon beam from the source to the detector, adequate experimental precautions must be taken to effectively minimise the response of the detector to photons whose energy is smaller than the primary photon energy. Using the high energy resolution

detectors, the detector system can be set to accept only the primary photons by regulating the bias of the detector system. The detector system employed in the present work is shown in the Fig.3.2. The scintillation counter used is a 1 in.dia.by 1 in.thick NaI(Tl) crystal mounted on a RCA 6199 photomultiplier tube. It was shielded by 2.5 cm lead. In this system the single channel analyzer (SCA) imposes a threshold amplitude (energy E) and a upper amplitude (E + ΔE) requirement on the output pulses from the linear amplifier. The pulse heights must lie between these two limits, as chosen by the lower voltage level control(E control) and the upper voltage level control (window width ΔE control) of the SCA. Thus the detector system can be set for monoenergetic primary photons, as evidenced from the appearance of the photo peak of the primary photon spectrum in the window.

Measurements of resolution of the system were made at the various photon energies used. The measured resolution at Co^{60} - 1332 KeV is 8% for full width at half maximum of the photo peak.

3.2.5. Gamma sources.

The description of the gamma ray sources used in the measurements is given in the table 3.3

TABLE 3.3

Source	Active size(approx.)	Physical form	Half-life	Approx. strength (mCi)	Photon energy MeV
Cs-137	4mm.dia. x 3mm long	Sealed source	30 y	20	0.662
Sc-46	4mm.dia. x 3mm long	Sealed source	84 d	130	0.889 1.120
Zn-65	4mm.dia. x 3mm.long	Sealed source	245 d	140	1.1155
Co-60	3mm.dia. x 2mm.long	Sealed source	5.3 y	100	1.173 1.332

3.2.6. Absorbers.

Measurements were made for 49 absorber materials which were at least 99.9% pure. 10 out of 49 materials were in elemental form (solid, liquid, powder). The remaining materials were chemical compounds. Most of these compounds were oxides. A few elements were studied in the form of halides, sulphates, and carbonates. Boron and nitrogen were in the form of boron carbide and boron nitride. Eleven scintillation grade hydrocarbons in liquid form were studied to derive the mean total attenuation cross section of hydrogen. The containers of liquid and powder samples were thin ($\sim$ 1 mm) perspex tube 1 cm internal diameter. Elaborate precaution was taken for uniform packing of powder sample in the container. The average thickness in g/cm^2 of each sample was determined from measurements of its area and weight.

As already mentioned, the maximum thickness of each sample was chosen in trial experiments to minimise the effect of multiple scattering.

3.3. Experimental procedure and measurements.

When the attenuation of the photon beam in the absorber is exponential, the total attenuation coefficient is given by the relation

$$I(x) = I_o e^{-\mu x} \tag{3.1}$$

where I_o is the beam intensity incident on the absorber slab, $I(x)$ is the intensity transmitted by the absorber, and x is the sample thickness in g/cm^2. In terms of transmission ratio $R = \frac{I(x)}{I_o}$ and absorber thickness x, μ (cm^2/g) is given by

$$\mu = \ln\left(\frac{1}{R}\right)/x \tag{3.2}$$

The attenuation coefficient is related to the total photon cross section (cm^2/atom) by

$$\mu = \sigma_t \times \frac{N}{A} \tag{3.3}$$

where N is Avogadro's number (6.02252×10^{23} atoms/g-atom) and A is the atomic weight of the absorber material. So, σ_t in barns/atom is given by

$$\sigma_t = \mu \Big/ \left(\frac{N}{A}\right) \times 10^{-24} \tag{3.4}$$

The values of the factor $(N/A) \times 10^{-24}$ for the elements studied are given in table A in Appendix.

For an absorber, the value of μ and hence σ_t can be obtained from the measurements of four quantities, namely the absorber thickness x, the incident beam intensity, the transmitted beam intensity and the background. If the absorber is a chemical compound the unknown total attenuation coefficient of any constituent element can be evaluated from the measured attenuation coefficient of the compound and the known coefficient of the other constituent elements using the equation

$$\mu_{comp} = \sum_i w_i \mu_i \tag{3.5}$$

where w_i is the proportion by weight of the ith constituent and μ_i is the attenuation coefficient of the ith constituent.

If a number of transmission measurements are made for a given sample thickness at a particular γ-ray energy, the attenuation coefficient can be calculated using the mean value of R and the average sample thickness x. The standard deviation S_μ of the measured value of μ interms of the standard deviation S_R of R and S_x of x is given by

$$S_\mu^2 = \left(\frac{\partial \mu}{\partial R}\right)^2 S_R^2 + \left(\frac{\partial \mu}{\partial x}\right)^2 S_x^2 \tag{3.6}$$

If for the same sample, the measurements is repeated at more than one thickness at the same energy by maintaining the exponential attenuation condition, a mean value of μ can be evaluated with the standard deviation of the mean value given by

$$\bar{S}_\mu^2 = \frac{1}{n^2} \sum_i S_{\mu,i}^2 \tag{3.7}$$

where $S_{\mu,i}$ is the standard deviation of μ obtained for the ith thickness of the sample.

3.3.1. Procedure.

The detector system was first set for a particular primary photon energy in the manner described in section 3.2.4. The thereshold bias control and the upper level control were set such that the SCA window covered the full photopeak width just above its half maximum. These settings were recorded as a function of time for a week to determine the long term stability of the electronics. It was found that the drift of the photopeak was negligibly small in 24 hours. The system was calibrated for energy and recalibration once a week was done during the whole course of measurements. During measurements with each sample at each energy, the photopeak position in the SCA window was checked and rechecked as a precaution against any fluctuation.

A holder was used to place the absorber sample in position normal to the beam. The holder could be moved with respect to the direction of the incident beam so that the different parts of the sample area could be exposed to the incident beam.

With the sample in position and a 20 cm lead stopper between the collimators No. 4 and 5 the mean background count rate was determined (1) when the source was not in its place and (2) when the source was in position. Using the strongest source (Zn-65, 140 mCi) used these counts per 4 hours were found to be 10680 and 10831 respectively. These data demonstrate the effectiveness of the shields and the collimators in preventing any rise in background in actual measurements.

When measuring with liquid or powder samples, the count with the empty container was taken for the no 'absorber' count to take into account any contribution to attenuation by the container itself.

For each thickness of sample, the counts for the same time was taken successively in the following order: background count, count without absorber, count with absorber, background count , count without absorber, count with absorber and so on. Each absorber count was taken after slightly moving the absorber such that the beam fell on slightly different position on the absorber area.

Counting times from 30 minutes to 5 hours were used to reduce the statistical error to 0.1 - 0.3%. For each sample, the measurements were repeated for two to three different thicknesses. The whole procedure is exemplified in table 3.4. The validity of exponential attenuation is evident from these data.

TABLE 3.4

Typical procedure for obtaining the results and the corresponding errors(The first significant figure in the fourth decimal place in standard deviations is shown).

Sample	Average sample thickness (gm/cm^2)	γ -ray energy 1.115 MeV.				
		1/R	μ (cm^2/gm)	S_μ	Average μ (cm^2/gm)	$\bar{S}_\mu$
	5.329	1.3805	0.0605	3		
S	7.106	1.5372	0.0605	3	0.0605	1
	9.682	1.7964	0.0605	2		
	12.960	2.1906	0.0605	2		

TABLE 3.4(Contd.)

Sample	Average sample thickness (gm/cm^2)	1/R	μ (cm^2/gm)	S_μ	Average μ (cm^2/gm)	S_μ
			γ-ray energy 1.115 MeV			
Ge	9.613	1.6966	0.0550	5	0.0549	2
	20.60	3.0639	0.0548	5		
	25.68	4.0829	0.0548	4		
Hg	29.12	6.254	0.0630	1	0.0630	1
	33.86	8.4413	0.0630	1		
			γ-ray energy 1.173 MeV			
Ge	5.084	1.3137	0.0532	3	0.0532	1
	9.613	1.6736	0.0533	1		
	20.60	2.9938	0.0532	1		
	35.297	6.5434	0.0532	1		

3.3.2. Measurements.

(i) Effect of geometry of the experimental setup on the measurements.

A set of measurements has been made to study the effect of geometry factor at different source-to-absorber distances. These distances were: 40 cm, 55 cm, 75 cm, 100 cm. The measured attenuation coefficients of germanium for Co-60 photons are given in the table 3.5. The data do not show any variation with solid angle.

TABLE 3.5

Measured attenuation coefficients in cm^2/gm of germanium for different maximum solid angles of the scattering cone from absorber to detector. (In parentheses is given the uncertainty in the last decimal place).

Solid angle (sr)	γ-ray energy 1.173 MeV	1.332 MeV
10.7×10^{-6}	0.0531(1)	0.0495(2)
13.3×10^{-6}	0.0530(1)	0.0493(2)
19.5×10^{-6}	0.0532(2)	0.0495(2)

(ii) Effect of multiple scattering on the measurements.

Some measurements have been made to study the effect of multiple scattering in the absorber as a function of absorber thickness. These were carried out with samples at 55 cm from the source, the solid angle between the absorber and the detector being 13.3×10^{-6}sr. The photopeak of the primary photon spectrum was scanned with 1 v window-width first without absorber and then with the absorber for one to three thicknesses. The spectra obtained for mercury are shown in Fig. 3.3 - 3.6. The attenuated spectra above certain absorber thickness exhibit the effect of multiple scattering, the FWHM being increased slightly over that for the incident spectrum. The attenuation coefficients determined for thicknesses at which the FWHM, of the photopeak remained almost the same are given in table 3.4 and 3.6.

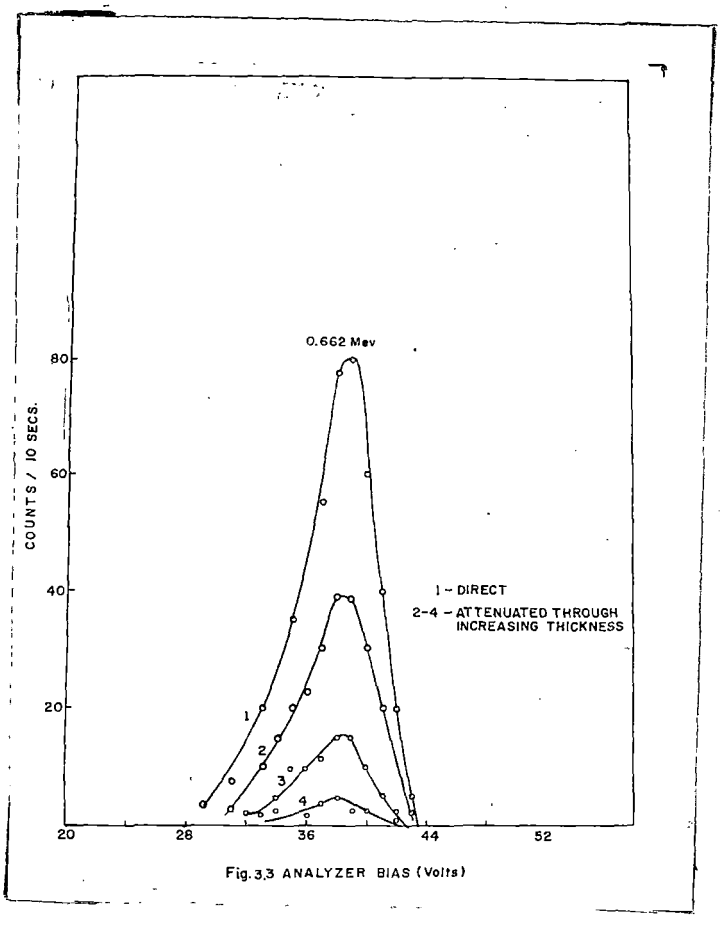

Fig. 3.3 ANALYZER BIAS (Volts)

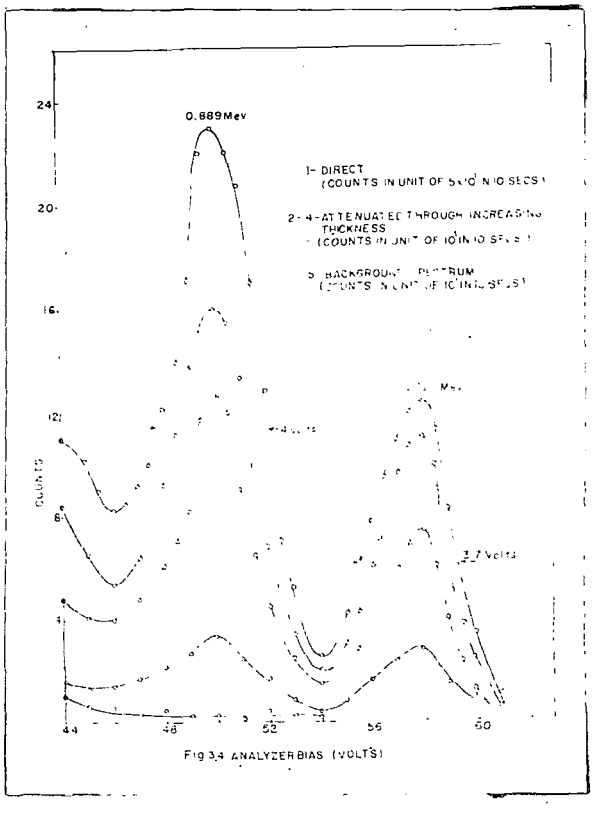

Fig 3.4 ANALYZER BIAS (VOLTS)

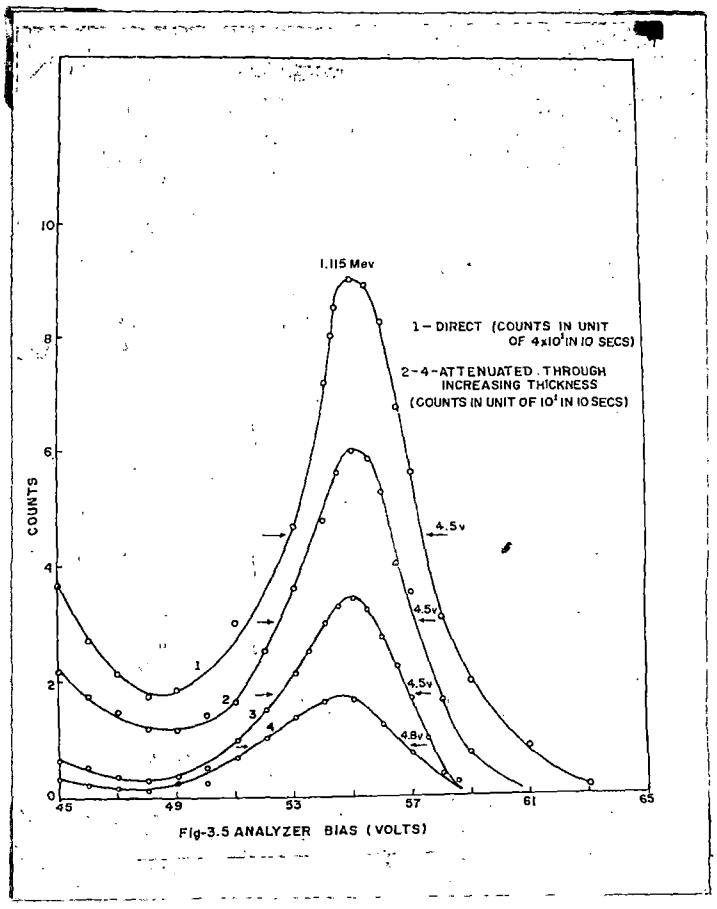

Fig-3.5 ANALYZER BIAS (VOLTS)

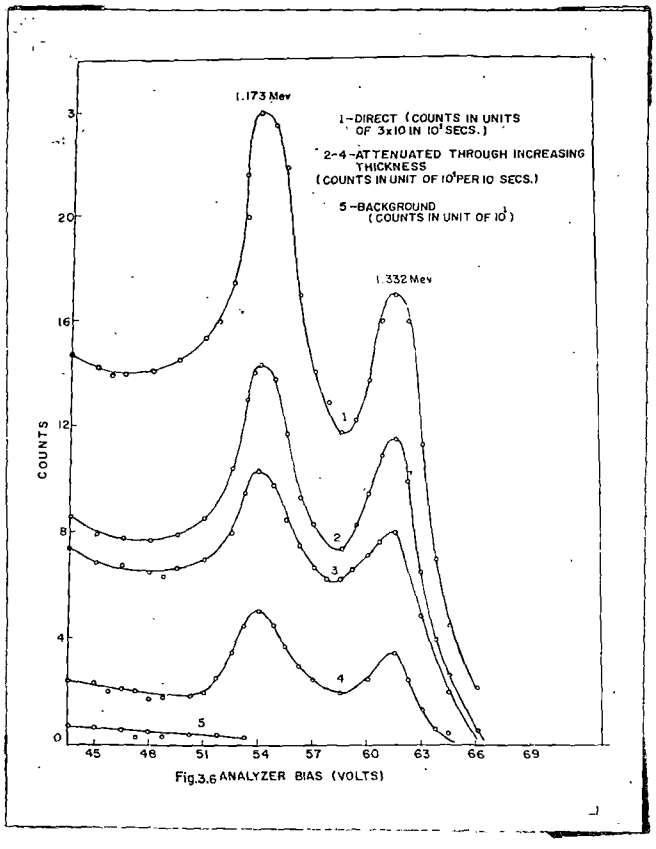

Fig.3.6 ANALYZER BIAS (VOLTS)

TABLE 3.6

Measured attenuation coefficients in cm^2/gm of mercury at varying thickness.

Thickness (gm/cm^2)	γ-ray energy(MeV) 0.889	1.115	1.120	1.173	1.332
29.12	0.0771(1)	0.0630(1)	0.0624(1)	0.0600(1)	0.0550(1)
33.86	0.0770(1)	0.0630(1)	0.0624(1)	0.0600(1)	0.0551(1)

(iii) Attenuation data.

The total attenuation data was obtained from measurements made at a solid angle of 13.3×10^{-6}sr between the absorber and the detector. The average thickness of a sample was determined to an accuracy of 0.05%. The mean attenuation coefficient of hydrogen was derived (table 3.7) from the measured attenuation data of hydrocarbons and carbon. The mean attenuation coefficient of oxygen (table 3.8) was derived following the same procedure by making measurements on the following set of samples: Al and Al_2O_3, Zn and ZnO, scintillation grade toluene and anisole, ethyl alcohol and ethane diol. The similar procedure was adopted to derive the attenuation data of elements from measurements on their compound.

TABLE 3.7

Typical procedure for obtaining the mass attenuation coefficient and total cross section for Hydrogen from the measured values of attenuation coefficients of scintillation grade hydrocarbons and carbon (μ_c = 0.0601 cm^2/gm) at γ -ray energy 1.115 MeV.

Organic compound		Mol. wt.	Fraction by wt.of C	Fraction by wt.of H	Measured attenuation coefficient of the compound μ	Attenuation coefficient of Hydrogen	Mean value $\bar{\mu}_H$	Cross section
Name	Formula	(gm/gm-mol.)	w_C	w_H	(cm^2/gm)	μ_H (cm^2/gm)	(cm^2/gm)	(barns/atom)
Toluene	$C_6H_5CH_3$	92.14	0.9125	0.0875	0.0653(1)	0.1208(1)		
O-xylene	$C_6H_4(CH_3)_2$	106.168	0.9051	0.0949	0.0657(1)	0.1203(1)		
Benzene	C_6H_6	78.114	0.9226	0.0774	0.0646(1)	0.1198(1)		
P-Cymene	$CH_3C_6H_4CH(CH_3)_2$	134.22	0.8949	0.1051	0.0663(1)	0.1200(1)		
Cyclohexane	C_6H_{12}	84.162	0.8563	0.1437	0.0686(1)	0.1201(1)		
Decalin	$C_{10}H_{18}$	138.254	0.8688	0.1312	0.0680(1)	0.1210(1)	0.1211(3)	0.2026(5)
Mesitylene	$(CH_3)_3C_6H_3$	120.20	0.8993	0.1007	0.0664(1)	0.1239(1)		
Ethylbenzene	$C_2H_5C_6H_5$	106.17	0.9050	0.0949	0.0659(1)	0.1220(1)		
n-butyl benzene	$C_{10}H_{14}$	134.22	0.8949	0.1051	0.0666(1)	0.1226(1)		
Cumene	$C_6H_5CH(CH_3)_2$	120.19	0.8993	0.1007	0.0660(1)	0.1200(1)		
P-xylene	$C_6H_4(CH_3)_2$	106.168	0.9051	0.0949	0.0658(1)	0.1214(1)		

TABLE 3.8

Procedure for obtaining the attenuation coefficient and cross section for Oxygen.

Energy (MeV)	Element used.	Compound used.	Measured attenuation coeff. of the element (cm^2/gm)	Measured attenuation coeff. of the compound (cm^2/gm)	Fraction by wt. of the element in the compound.	Fraction by wt. of oxygen in the compound.	Mol. wt. of the compd. (gm/gm-mol.)	Attenuation coeff. of oxygen (cm^2/gm)	Cross section for oxygen (barns/atom)
	Zn	ZnO	0.0561(1)	0.0570(1)	0.8034	0.1966	81.38	0.0605(2)	1.61(1)
	Al	Al_2O_3	0.0583(2)	0.0594(1)	0.5293	0.4708	101.94	0.0603(2)	1.60(1)
1.115	H	H_2O	0.121(03)	0.0672(1)	0.1119	0.8881	18.016	0.0605(3)	1.61(1)
		Toluene*		0.0653(1)			92.14		
		Anisole**		0.0648(1)		0.1479	108.13	0.0615(3)	1.63(1)

* Fraction by weight of the constituent elements are given in table 3.7.

**Fraction by weight of the constituent elements:- $w_C = 0.7768$, $w_O = 0.1479$, $w_H = 0.0746$

3.4. Evaluation of uncertainties in measurements.

The procedure of obtaining the final errors to the measured attenuation coefficients by combining the estimated experimental errors is shown in the table 3.4. These experimental errors are the standard deviation of the set of transmission ratios and the standard deviation of the set of measured thickness values. Attempt has been made in every step to maintain a relatively low level of statistical uncertainty.

In obtaining the attenuation coefficient of As at Cs-137-0.662 MeV from the measured attenuation coefficients of As_2O_3 and oxygen, the maximum experimental error was 2.5%, estimated by quadratically combining the statistical error arising at each step of the whole process. A possible experimental error due to point-to-point variation of sample thickness has been minimised in the course of measurement by taking transmission count at a number of positions over the area of each sample. Sample impurity error was kept to a minimum by choosing high purity samples.

As has already been outlined in the section 3.1, considrations have been made so that corrections were not necessary for some of the systematic errors arising in the narrow-beam transmission experiment. In the following we shall discuss in detail systematic errors we have taken into account in the present set of measurements:

(a) The detector detects some of the photons scattered at very small angles and other secondary radiations (bremsstrahlung, annihilation photons) introduced in the absorber.

Incoherently Compton scattered photons, at small angle, suffer an energy change so small that the detector cannot resolve them from the primary photons. Coherent Rayleigh scattered photons have nearly the same energy as the primary photons. Tarrant (Ta 30) made an analysis of the

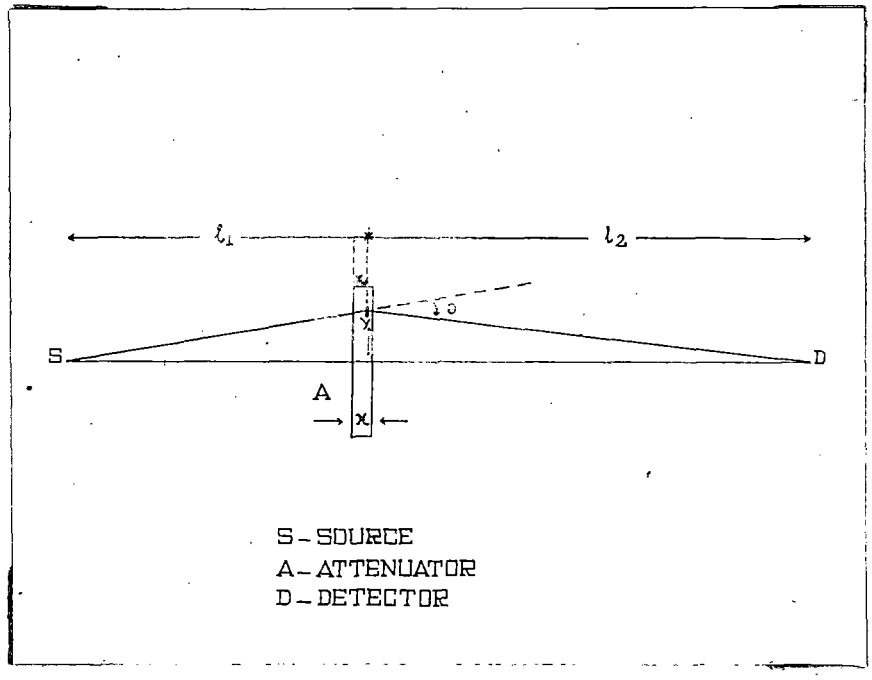

Fig. 3.7

situation in the geometry (Fig.3.7) of the narrow-beam transmission experiment and obtained for the number of photons scattered at an angle θ to the detector, the equation

$$n_s = \frac{I_0 A \epsilon}{(l_1+l_2)^2} N x e^{-\mu x} \sigma_{\theta_0} \tag{3.8}$$

$$\sigma_{\theta_0} = \int_0^{\theta_0} \sigma(\theta) d\Omega = 2\pi \int_0^{\theta_0} \sigma(\theta) \sin\theta \, d\theta \tag{3.9}$$

Since, in the same geometry the number of primary photons transmitted and detected by the detector is

$$I = \frac{I_0 A \epsilon}{(l_1+l_2)^2} e^{-\mu x} \tag{3.10}$$

the ratio of the number of scattered to the number of transmitted photons is

$$n_s/I = N x \sigma_{\theta_0} \tag{3.11}$$

Here, I_0 is the number of photons per unit solid angle emmitted by the source per second, μ is the attenuation coefficient of the primery photons, ϵ is the efficiency of the detector for primary photons, N is the number of atoms per unit volume in the absorber, A is the area of the detector and

$$\sigma(\theta) = d\sigma(\theta)/d\Omega$$

is the sum of differential incoherent scattering cross section $\sigma_{INCOH}(\theta)$ and the differential coherent Rayleigh scattering cross section $\sigma_{COH}(\theta)$. θ_0 is the maximum angle of scattering for photons reaching the detector.

For Compton scattering, $\sigma_{INCOH}(\theta)$ is the Klein-Nishina differential cross section per atom and the cross section $\sigma^c_{\theta_0}$ for the number of Compton scattered photons in the angular interval 0 to θ_0, when θ_0 approaches zero becomes,

$$\sigma^c_{\theta_0} = Z\left(\pi r_0^2 \theta_0^2\right) \tag{3.12}$$

where θ_0 is in radian, Z is the atomic number of the scatterer atom.

This shows that for small angle, the number of Compton scattered photons reaching the detector is proportional to the solid angle of the collimating system. Coherent Rayleigh scattering cross section $\sigma^R_{\theta_0}$, for the number of Rayleigh scattered photons in the angular interval 0 to θ_0 was calculated numerically using, through interpolation at small angle, the calculated differential scattering cross section data of Brown(B 66). These results and the calculated values of σ^c_θ from Davisson and Evans (Da 52) and the corresponding ration n_s/I estimated for a selected Pb sample thickness and energies are shown in the table 3.9. The data show that within a maximum angle of 30', contributions from the single Compton and Rayleigh scattering are negligible and corrections to the data are not necessary for this effect.

It can also be seen that the effect of some of the secondary radiation such as bremsstrahlung, produced in the absorber and reaching the detector would be much less than that from the primary process of single photon scattering.

TABLE 3.9

Some results estimated using equation 3.11.

Element	Nx (atoms/cm^2)	$\sigma^c_{\theta_0}$ (cm^2/atom)	$\sigma^R_{\theta_0}$ (cm2/atom)	$\sigma^c_{\theta_0}+\sigma^R_{\theta_0}$ (barns/atom)	n_s/I
Pb	5.498×10^{22}	1.55×10^{-27}	0.0574×10^{-24}	0.0590	0.00324
Al	3.48×10^{23}	0.24×10^{-27}	0.336×10^{-27}	0.000583	0.00020

(b) The detector detects some multiply scattered photons from the absorber.

In measurements with thick absorbers, some of the singly scattered photons which have been considered as lost in deriving the ratio n_s/I may be scattered and rescattered in the absorber. Some of these photons may be reach the detector, although their number would be much less than the number of singly scattered photons. Precautions have been taken to minimise the effect by (i) making the incident collimated beam intercept a very small area of the absorber (ii) collimating the beam narrowly upto the detector and (iii) making measurements at relatively thin samples- chosen in the manner described in the section 3.2.3.

(c) The detector detects at the photopeak energy of one γ-ray some other γ-rays close in energy.

The effect arises due to 8 - 10% resolution near 1 MeV of the NaI(Tl) detector system. For measurements at 1.173 and 1.332 MeV with Co-60 source, and at 0.889 and 1.120 MeV with Sc-46 source, corrections to be applied to the data were determined experimentally by the following method adopted by Colgate (Co 52). The FWHM of Co-60 1.173 MeV photopeak was determined to be 4 volts. The detector system with the analyzer window of 4 volts was set on the photopeak of Zn-65 1.115 MeV (the energy being very close to 1.173 MeV) and the mean counting rate was determined. The analyzer bias was then shifted to a higher level by an amount equal to the energy difference 0.159 MeV between 1.332 and 1.173 MeV and the mean counting rate determined with the same window. The second rate gives the number of 1.115 MeV photons counted at an energy difference 0.159 MeV on the photopeak of 1.274 MeV. The ratio of the count rate at 1.274 MeV to that at 1.115 MeV was taken as the relative contribution of one photopeak to the other. Experimentally found value for this relative contribution was 2%. The procedure was repeated with Mn-54(0.840MeV) source for measurements with Sc-46 source.

The relative contribution for two energies 0.889 and 1.120 was 1%.

(d) Effect of energy degradation of primary photons due to Compton scattering in the source material.

Compton scattering of primary photons in the source material changes the energy of photons. The magnitude of the effect can be minimised by choosing small sources and narrowly collimating the source. The effect was found too small for the present measurements at very small angles with the available small sources to affect the data.

(e) The counting system loses some counts at high counting rate due to its finite resolving time.

The resolving time of the counting setup experimentally determined by standard method was 10 μ sec. The direct count rate varied from 25/sec. to 729/sec. So the count loss correction was small and taken into consideration in the analysis.

(f) Effect of background scattering.

As already mentioned in the section 3.3.1, the actual background counts during all the measurements were small. The background spectrum in the measurements are shown in the figs.3.4, 3.6. The direct and transmitted counts were corrected for the background count taken in the manner discussed before.

3.5. Evaluation of the cross sections.

The total attenuation coefficients calculated using equation(3.2) and those obtained using equation (3.5) and the table (D) in Appendix are listed in the table 3.10. For their interpretation in relation to atomic number Z, the data have been converted to total cross sections using equation 3.4. Table 3.11 contains these total cross sections.

3.5.1. Evaluation of total scattering cross sections.

Total attenuation cross sections, in the low and intermediate atomic number regions, near 1 MeV are negligibly affected by photoelectric absorption process. At 1 MeV the photoelectric absorption begins to influence total cross sections at Z = 70 until it contributes a significant proportion at Z = 80 (total scattering cross section is 18 barns/atom approx.; total photoelectric cross section 6.4 barns/atom approx.). At 600 KeV, the photoelectric cross section becomes a significant proportion of total cross section at Z = 80. Between 1.02 MeV and 1.4 MeV, the contribution of pair production process to total attenuation is also negligible for all elements upto Z = 92. This means that the minor contributions of photoelectric & pair production processes in the appropriate regions can be treated as corrections to the measured total cross sections to evaluate the total scattering cross sections.

A. Corrections for photoelectric effect.

In this connection we mention some new extensive theoretical results for photoelectric cross section given by the Rakavy and Ron (Ra 67), Schmickley and Pratt (Sc 67) and Scofield (Sc73). These results have been obtained using relativistic calculations which included the effects of screening of the nuclear charge by the other atomic electrons which are treated relativistically. Rakavy and Ron calculated cross sections for Z=12, 26, 50, 74 and 92 in the energy range 1 to 2000 KeV. Schmickley and Pratt's results covered 14 elements between Z = 13 and Z = 92 in the energy range 10 - 3000 KeV. Scofield has calculated cross sections to an accuracy of 1 to 3% for all elements Z = 1 to 101 in the energy range 1 to 1500 KeV.

Using Scofield's values of total photoelectric cross sections to interpolate at each energy of the present work, correction for photoelectric effect to be subtracted from the measured total cross section was evaluated. These corrections are given in the second column of the table 3.11.

B. Correction for pair production.

For high Z elements, a pair production correction is necessary at energies above the threshold (1.022 MeV) in the energy range of the present work.

This correction was estimated by interpolation of the exactly calculated pair production cross sections of Øverbo (Ø70) for a large number of photon energies in the range 1.022 to 5.11 MeV. These corrections when significant are shown in the third column of table 3.11.

The final results for the total scattering cross sections are shown in the last column of table 3.11.

TABLE 3.10

Measured total attenuation coefficients in cm^2/gm (In parentheses is given the uncertainty in the last one or two places).

Element	Z	γ-ray energy (MeV)		
		0.662	0.889	1.115
H	1	0.153(2)	0.134(1)	0.121(1)
Li	3	0.0659(8)	0.0592(2)	0.0583(2)
B	5	0.0703(8)	0.0624(2)	0.0568(2)
C	6	0.0771(6)	0.0673(1)	0.0601(1)
N	7	0.0782(9)	0.0674(3)	0.0605(3)
O	8	0.0780(12)	0.0675(2)	0.0604(2)
F	9	0.0742(8)	0.0650(2)	0.0608(2)
Na	11	0.0735(7)	0.0652(3)	0.0572(3)
Mg	12	0.0762(8)	0.0659(3)	0.0597(3)
Al	13	0.0744(14)	0.0647(2)	0.0583(2)
Si	14	0.0776(12)	0.0673(3)	0.0604(2)
S	16	0.0783(6)	0.0680(1)	0.0605(1)
K	19	0.0768(8)	0.0659(2)	0.0586(2)
Ca	20	0.0781(14)	0.0677(3)	0.0601(3)
Ti	22	0.0716(13)	0.0624(3)	0.0556(3)
Fe	26	0.0731(4)	0.0635(1)	0.0568(1)
Zn	30	0.0730(6)	0.0630(1)	0.0561(1)

TABLE 3.10(CONTD.)

Element	Z	γ -ray energy (MeV)		
		0.662	0.889	1.115
Ge	32	0.0723(4)	0.0614(1)	0.0549(1)
As	33	0.0708(18)	0.0607(3)	0.0543(3)
Br	35	0.0710(6)	0.0605(1)	0.0539(1)
Rb	37	0.0704(13)	0.0603(3)	0.0534(3)
Mo	42	0.0734(13)	0.0618(3)	0.0549(3)
I	53	0.0772(4)	0.0630(1)	0.0543(1)
Cs	55	0.0775(6)	0.0627(2)	0.0542(2)
Ba	56	0.0771(8)	0.0622(2)	0.0536(2)
La	57	0.0784(13)	0.0630(2)	0.0542(3)
Ce	58	0.0798(13)	0.0639(2)	0.0550(3)
Nd	60	0.0824(13)	0.0656(2)	0.0561(3)
Sm	62	0.0838(13)	0.0659(2)	0.0562(3)
Gd	64	0.0850(13)	0.0663(2)	0.0563(3)
Dy	66	0.0871(13)	0.0672(3)	0.0570(3)
Yb	70	0.0922(13)	0.0695(3)	0.0585(3)
Hg	80	0.1061(1)	0.0771(1)	0.0630(1)
Pb	82	0.1072(1)	0.0784(1)	0.0640(1)

TABLE 3.10 (CONTD.)

Element	Z	γ -ray energy (MeV)		
		1.120	1.173	1.332
H	1	0.120(1)	0.120(1)	0.110(1)
Li	3	0.0522(2)	0.0509(2)	0.0489(2)
B	5	0.0562(2)	0.0536(2)	0.0508(2)
C	6	0.0603(1)	0.0585(1)	0.0551(1)
N	7	0.0603(3)	0.0588(3)	0.0552(3)
O	8	0.0602(2)	0.0589(2)	0.0551(2)
F	9	0.0582(2)	0.0560(2)	0.0520(2)
Na	11	0.0571(3)	0.0560(3)	0.0530(3)
Mg	12	0.0590(3)	0.0577(3)	0.0536(3)
Al	13	0.0576(2)	0.0567(2)	0.0531(2)
Si	14	0.0602(2)	0.0589(2)	0.0551(2)
S	16	0.0598(1)	0.0592(1)	0.0555(1)
K	19	0.0589(2)	0.0576(2)	0.0540(2)
Ca	20	0.0601(3)	0.0595(3)	0.0559(3)
Ti	22	0.0555(3)	0.0546(3)	0.0509(3)
Fe	26	0.0571(1)	0.0557(1)	0.0521(1)
Zn	30	0.0562(1)	0.0548(1)	0.0511(1)

TABLE 3.10(CONTD.)

Element	Z	γ -ray energy (MeV)		
		1.120	1.173	1.332
Ge	32	0.0552(1)	0.0532(1)	0.0495(1)
As	33	0.0539(3)	0.0529(3)	0.0492(3)
Br	35	0.0537(1)	0.0528(1)	0.0494(1)
Rb	37	0.0532(3)	0.0520(3)	0.0489(3)
Mo	42	0.0548(3)	0.0535(3)	0.0501(3)
I	53	0.0543(1)	0.0526(1)	0.0499(1)
Cs	55	0.0541(2)	0.0530(2)	0.0494(2)
Ba	56	0.0535(2)	0.0521(2)	0.0489(2)
La	57	0.0541(3)	0.0527(3)	0.0493(3)
Ce	58	0.0548(3)	0.0534(3)	0.0499(3)
Nd	60	0.0560(3)	0.0547(3)	0.0520(3)
Sm	62	0.0561(3)	0.0547(3)	0.0507(3)
Gd	64	0.0562(3)	0.0551(3)	0.0508(3)
Dy	66	0.0569(3)	0.0560(3)	0.0513(3)
Yb	70	0.0583(3)	0.0566(3)	0.0527(3)
Hg	80	0.0624(1)	0.0600(1)	0.0550(1)
Pb	82	0.0640(1)	0.0615(1)	0.0557(1)

TABLE 3.11

Measured cross sections(barns/atom) obtained in the present work.(The number in parentheses is the uncertainty in the last decimal place. Corrections are shown after rounding off, to the third decimal place. No correction is shown if there is no significant figure in the third decimal place of correction).

Z	γ-ray energy (MeV) 0.662			0.869		
	Total	Photoelectric absorption correction	Scattering	Total	Photoelectric absorption correction	Scatter
1	0.256(3)	—	0.256(3)	0.224(2)		0.224(2
3	0.759(10)		0.759(10)	0.682(2)		0.682(2
5	1.26(1)		1.26(1)	1.12(4)		1.12(4
6	1.54(1)		1.54(1)	1.34(0)		1.34(0
7	1.82(2)		1.82(2)	1.57(1)		1.57(1
8	2.07(3)		2.07(3)	1.79(1)		1.79(1
9	2.34(2)		2.34(2)	2.05(1)		2.05(1
11	2.81(3)	0.001	2.81(3)	2.49(1)	0.001	2.49(1
12	3.08(3)	0.002	3.08(3)	2.66(1)	0.001	2.66(1
13	3.33(3)	0.003	3.33(3)	2.90(1)	0.002	2.90(1
14	3.62(3)	0.004	3.62(3)	3.14(1)	0.002	3.14(1
16	4.16(3)	0.007	4.15(3)	3.61(1)	0.004	3.61(1

TABLE 3.11 (Contd.)

Z	γ-ray energy (MeV) 0.662			0.889		
	Total	Photoelectric absorption correction	Scattering	Total	Photoelectric absorption correction	Scatter
19	4.98(5)	0.018	4.96(5)	4.28(2)	0.009	4.27(2)
20	5.20(10)	0.023	5.18(10)	4.50(2)	0.012	4.49(2)
22	5.70(10)	0.036	5.66(10)	4.96(2)	0.018	4.94(2)
26	6.78(4)	0.080	6.70(4)	5.88(1)	0.041	5.84(1)
30	7.92(6)	0.154	7.77(1)	6.84(1)	0.080	5.76(1)
32	8.71(5)	0.223	8.49(5)	7.40(1)	0.109	7.29(1)
33	8.81(2)	0.236	8.57(2)	7.55(4)	0.122	7.43(4)
35	9.42(8)	0.310	9.11(8)	8.03(1)	0.158	7.87(1)
37	10.5(2)	0.391	10.1(2)	8.56(4)	0.203	8.36(4)
42	11.7(2)	0.735	11.0(2)	9.84(5)	0.380	9.46(5)
53	16.3(1)	2.11	14.2(1)	13.27(2)	1.09	12.18(2
55	17.1(1)	2.48	14.6(1)	13.84(4)	1.28	12.56(4
56	17.6(2)	2.69	14.9(2)	14.18(5)	1.39	12.79(5
57	18.1(3)	2.91	15.2(3)	14.53(5)	1.51	13.02(5
58	18.6(3)	3.14	15.5(3)	14.87(5)	1.63	13.24(5
60	19.7(3)	3.70	16.0(3)	15.71(5)	1.93	13.78(5
62	20.9(3)	4.28	16.6(3)	16.45(5)	2.23	14.22(5
64	22.2(4)	4.92	17.3(4)	17.31(5)	2.57	14.74(5
66	23.5(4)	5.64	17.9(4)	18.13(1)	2.95	15.18(1
70	26.5(4)	7.32	19.2(4)	20.0(1)	3.84	16.2(1)
80	35.34(3)	13.32	22.0(3)	25.68(3)	7.04	18.64(3
82	36.90(3)	14.90	22.0(3)	26.96(3)	7.86	19.10(3

TABLE 3.11 (Contd.)

Z	γ-ray energy 1.115 (MeV)			
	Total	PEAC	PPAC	Scattering
1	0.202(2)			0.202(2)
3	0.615(2)			0.615(2)
5	1.02(4)			1.02(4)
6	1.20(0)			1.20(0)
7	1.41(1)			1.41(1)
8	1.60(1)			1.60(1)
9	1.92(1)			1.92(1)
11	2.18(1)			2.18(1)
12	2.41(1)			2.41(1)
13	2.61(1)			2.61(1)
14	2.82(10)	0.001		2.82(1)
16	3.21(1)	0.002		3.21(1)
19	3.80(1)	0.006		3.79(1)
20	4.00(2)	0.007		3.99(2)
22	4.42(2)	0.011		4.41(2)
26	5.26(1)	0.026	0.001	5.23(1)
30	6.09(1)	0.050	0.001	6.04(1)
32	6.62(1)	0.069	0.001	6.55(1)

PEAC-Photoelectric absorption correction

PPAC-Pair production absorption correction

TABLE 3.11 (Contd.)

Z	γ-ray energy 1.115 (MeV)			
	Total	PEAC	PPAC	Scattering
33	6.76(4)	0.076	0.002	6.68(4)
35	7.15(1)	0.099	0.002	7.05(1)
37	7.58(4)	0.128	0.002	7.45(4)
42	8.75(5)	0.238	0.003	8.51(5)
53	11.44(2)	0.688	0.004	10.75(2)
55	11.96(4)	0.811	0.005	11.14(4)
56	12.22(5)	0.880	0.005	11.34(5)
57	12.5(1)	0.952	0.005	11.5(1)
58	12.8(1)	1.03	0.005	11.8(1)
60	13.4(1)	1.21	0.006	12.2(1)
62	14.0(1)	1.40	0.006	12.6(1)
64	14.7(1)	1.62	0.006	13.1(1)
66	15.4(1)	1.86	0.006	13.5(1)
70	16.8(1)	2.42	0.007	14.4(1)
80	21.00(3)	4.47	0.008	16.52(3)
82	22.02(3)	4.97	0.008	17.04(3)

PEAC-Photoelectric absorption correction

PPAC-Pair production absorption correction

TABLE 3.11 (Contd.)

Z	γ-ray energy 1.120 (MeV)			
	Total	PEAC	PPAC	Scattering
1	0.201(2)			0.201(2)
3	0.601(2)			0.601(2)
5	1.01(4)			1.01(4)
6	1.20(2)			1.20(2)
7	1.40(1)			1.40(1)
8	1.60(1)			1.60(1)
9	1.84(1)			1.84(1)
11	2.18(1)			2.18(1)
12	2.38(1)			2.38(1)
13	2.58(1)			2.58(1)
14	2.81(1)	0.001		2.81(1)
16	3.18(1)	0.002		3.18(1)
19	3.82(1)	0.006		3.81(1)
20	4.00(2)	0.007		3.99(2)
22	4.42(2)	0.011		4.41(2)
26	5.29(1)	0.026	0.001	5.26(1)
30	6.10(1)	0.050	0.001	6.05(1)
32	6.65(1)	0.068	0.001	6.58(1)

PEAC-Photoelectric absorption correction

PPAC-Pair production absorption correction

TABLE 3.11(Contd.)

Z	γ-ray energy 1.20 (MeV)			
	Total	PEAC	PPAC	Scattering
33	6.71(4)	0.075	0.002	6.63(4)
35	7.12(1)	0.098	0.002	7.02(1)
37	7.55(4)	0.126	0.002	7.42(4)
42	8.73(5)	0.234	0.003	8.49(5)
53	11.44(2)	0.681	0.004	10.76(2)
55	11.94(4)	0.804	0.004	11.13(4)
56	12.20(5)	0.871	0.005	11.32(5)
57	12.5(1)	0.943	0.005	11.5(1)
58	12.8(1)	1.02	0.005	11.8(1)
60	13.4(1)	1.20	0.006	12.2(1)
62	14.0(1)	1.39	0.006	12.6(1)
64	14.7(1)	1.60	0.006	13.0(1)
66	15.41(1)	1.84	0.006	13.5(1)
70	16.8(1)	2.34	0.007	14.4(1)
80	20.79(3)	4.43	0.008	16.35(3)
82	22.02(3)	4.93	0.008	17.08(3)

PEAC-Photoelectric absorption correction

PPAC-Pair production absorption correction

TABLE 3.11 (Contd.)

Z	γ -ray energy 1.173 (MeV)			
	Total	PEAC	PPAC	Scattering
1	0.201(2)			0.201(2)
3	0.586(2)			0.586(2)
5	0.963(36)			0.963(36)
6	1.17(0)			1.17(0)
7	1.37(1)			1.37(1)
8	1.56(1)			1.56(1)
9	1.77(1)			1.77(1)
11	2.14(1)			2.14(1)
12	2.33(1)			2.33(1)
13	2.54(1)			2.54(1)
14	2.75(1)	0.001		2.75(1)
16	3.14(1)	0.002		3.14(1)
19	3.74(1)	0.005	0.001	3.73(1)
20	3.96(2)	0.007	0.001	3.95(2)
22	4.34(2)	0.010	0.002	4.33(2)
26	5.16(1)	0.024	0.002	5.13(1)
30	5.95(1)	0.046	0.003	5.90(1)
32	6.41(1)	0.060	0.004	6.35(1)

PEAC-Photoelectric absorption correction

PPAC-Pair production absorption correction

TABLE 3.11 (Contd.)

Z	γ-ray energy 1.173 (MeV)			
	Total	PEAC	PPAC	Scattering
33	6.58(4)	0.071	0.003	6.51(4)
35	7.00(1)	0.092	0.005	6.90(1)
37	7.38(4)	0.118	0.006	7.26(4)
42	8.52(5)	0.215	0.008	8.30(5)
53	11.08(2)	0.626	0.014	10.44(2)
55	11.70(4)	0.740	0.015	10.94(2)
56	11.88(5)	0.802	0.015	11.06(5)
57	12.15(7)	0.869	0.016	11.26(7)
58	12.42(7)	0.940	0.017	11.46(7)
60	13.10(7)	1.12	0.018	11.96(7)
62	13.65(8)	1.29	0.020	12.34(8)
64	14.38(8)	1.49	0.021	12.87(8)
66	15.11(8)	1.71	0.023	13.38(8)
70	16.26(9)	2.23	0.026	14.00(9)
80	19.99(3)	4.05	0.034	15.91(3)
82	21.16(34)	4.52	0.035	16.60(3)

PEAC-Photoelectric absorption correction

PPAC-Pair production absorption correction

TABLE 3.11 (Contd.)

Z	γ-ray energy 1.332 (MeV)			
	Total	PEAC	PPAC	Scattering
1	0.184(2)			0.184(2)
3	0.563(2)			0.563(2)
5	0.91(36)			0.91(36)
6	1.10(0)			1.10(0)
7	1.28(1)			1.28(1)
8	1.46(1)		0.001	1.46(1)
9	1.64(1)		0.001	1.64(1)
11	2.02(1)		0.002	2.14(1)
12	2.16(1)		0.002	2.16(1)
13	2.38(1)		0.003	2.38(1)
14	2.57(1)	0.001	0.003	2.57(1)
16	2.95(1)	0.002	0.004	2.94(1)
19	3.50(1)	0.004	0.006	3.49(1)
20	3.72(2)	0.005	0.007	3.71(1)
22	4.05(2)	0.008	0.009	4.03(1)
26	4.83(1)	0.018	0.013	4.80(1)
30	5.55(1)	0.036	0.017	5.49(1)
32	5.97(1)	0.050	0.020	5.90(1)

PEAC-Photoelectric absorption correction

PPAC-Pair production absorption correction

TABLE 3.11 (Contd.)

Z	γ -ray energy 1.332 (MeV)			
	Total	PEAC	PPAC	Scattering
33	6.12(4)	0.055	0.022	6.04(4)
35	6.55(1)	0.072	0.025	6.45(1)
37	6.94(4)	0.093	0.030	6.82(4)
42	7.98(5)	0.171	0.047	7.76(5)
53	10.51(2)	0.493	0.073	9.94(2)
55	10.90(4)	0.583	0.080	10.24(4)
56	11.15(5)	0.632	0.085	10.43(5)
57	11.37(7)	0.685	0.090	10.60(7)
58	11.61(7)	0.741	0.093	10.78(7)
60	12.45(7)	0.867	0.102	11.48(7)
62	12.65(8)	1.01	0.111	11.53(8)
64	13.26(8)	1.16	0.122	11.98(8)
66	13.84(8)	1.33	0.135	12.38(8)
70	15.14(9)	1.74	0.154	13.25(9)
80	18.32(3)	3.18	0.220	14.92(3)
82	19.16(3)	3.55	0.235	15.37(3)

PEAC-Photoelectric absorption correction

PPAC-Pair production absorption correction

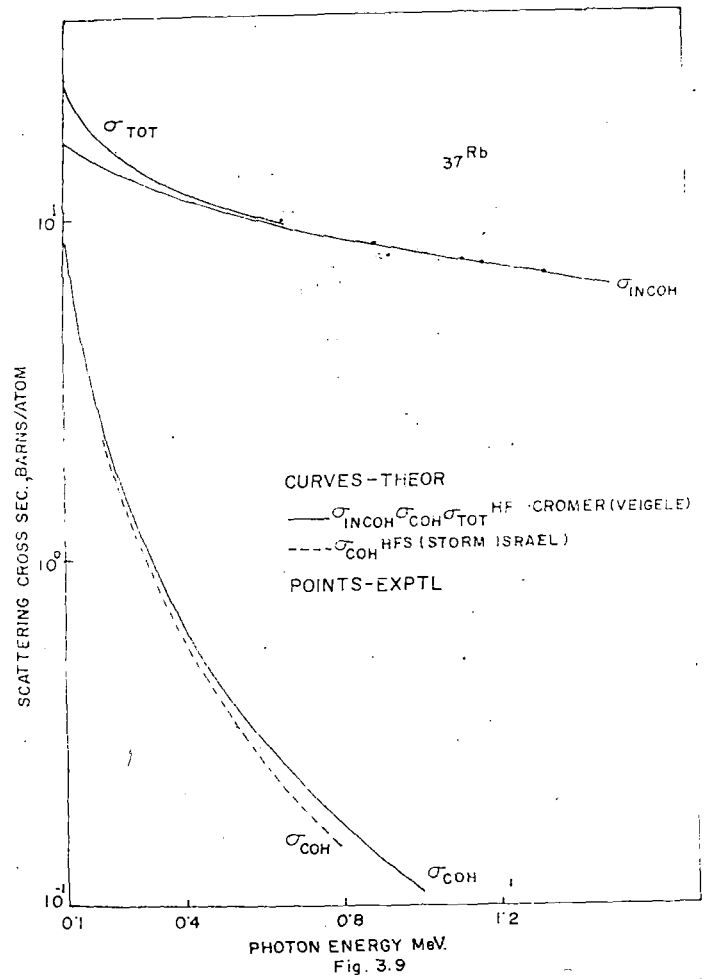
σ_{TOT}
$_{37}Rb$
10^1
σ_{INCOH}
SCATTERING CROSS SEC., BARNS/ATOM
CURVES-THEOR
$\sigma_{INCOH}\sigma_{COH}\sigma_{TOT}$ HF CROMER (VEIGELE)
σ_{COH} HFS (STORM ISRAEL)
POINTS-EXPTL
10^0
σ_{COH}
σ_{COH}
10^{-1}
0·1
0·4
0·8
1·2
PHOTON ENERGY MeV.
Fig. 3.9

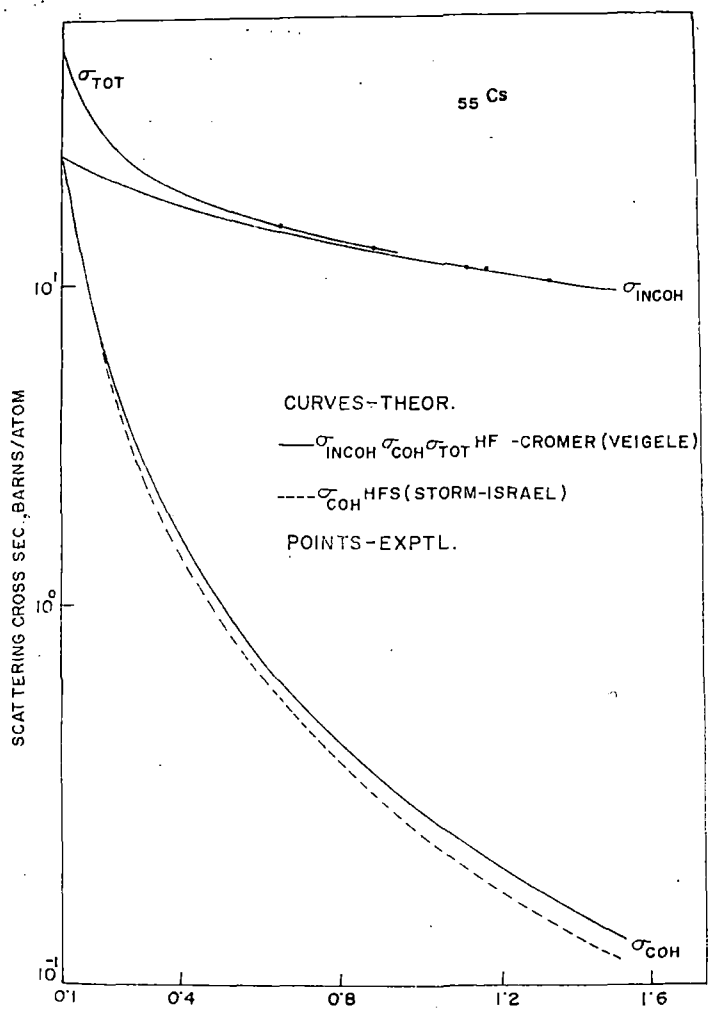
σTOT
55 Cs
σINCOH
CURVES-THEOR.
—σINCOH σCOH σTOT HF -CROMER (VEIGELE)
----σCOH HFS (STORM-ISRAEL)
POINTS-EXPTL.
σCOH
10¹
10⁰
10⁻¹
SCATTERING CROSS SEC., BARNS/ATOM
0·1
0·4
0·8
1·2
1·6
PHOTON ENERGY MeV.
Fig. 3.10

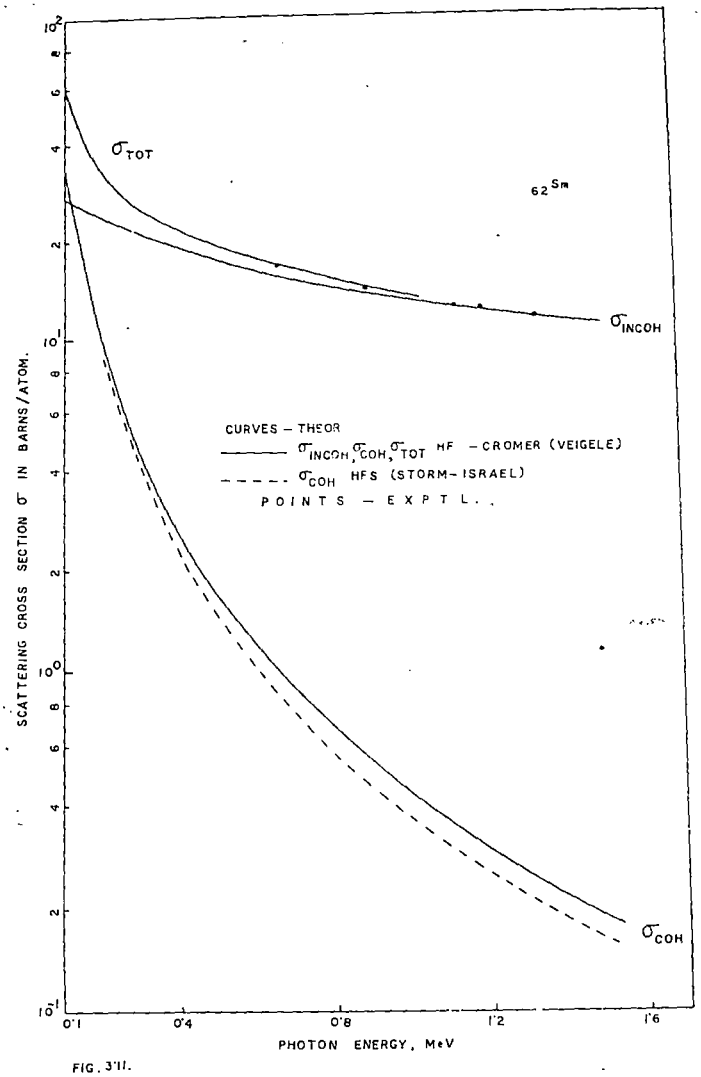
10^2
10^1
10^0
10^{-1}
σ_{TOT}
$_{62}Sm$
σ_{INCOH}
CURVES – THEOR
$\sigma_{INCOH}, \sigma_{COH}, \sigma_{TOT}$ HF – CROMER (VEIGELE)
σ_{COH} HFS (STORM–ISRAEL)
POINTS – EXPTL.
σ_{COH}
SCATTERING CROSS SECTION σ IN BARNS/ATOM.
0·1
0·4
0·8
1·2
1·6
PHOTON ENERGY, MeV

FIG. 3·11.

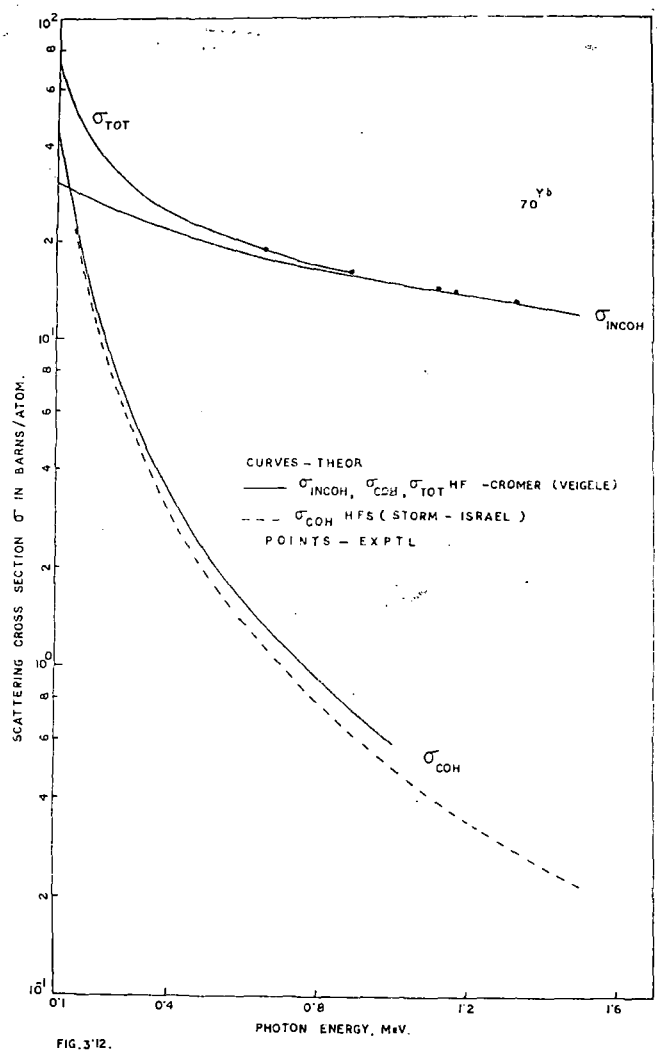
10^2
8
6
4
2
10^1
8
6
4
2
10^0
8
6
4
2
10^{-1}
σ_{TOT}
σ_{INCOH}
σ_{COH}
$_{70}Yb$
CURVES - THEOR
σ_{INCOH}, σ_{COH}, σ_{TOT} HF -CROMER (VEIGELE)
σ_{COH} HFS (STORM - ISRAEL)
POINTS - EXPTL
SCATTERING CROSS SECTION σ IN BARNS/ATOM.
0·1
0·4
0·8
1·2
1·6
PHOTON ENERGY, MeV.

FIG. 3·12.

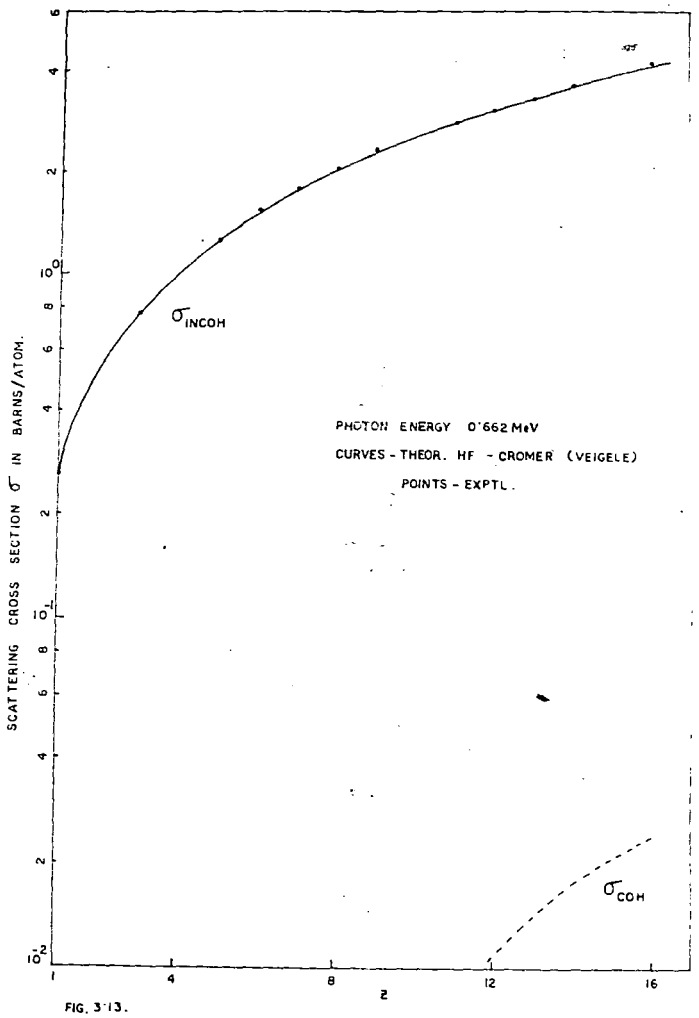
SCATTERING CROSS SECTION σ IN BARNS/ATOM.
σINCOH
σCOH
PHOTON ENERGY 0·662 MeV
CURVES - THEOR. HF - CROMER (VEIGELE)
POINTS - EXPTL.
Z

FIG. 3·13.

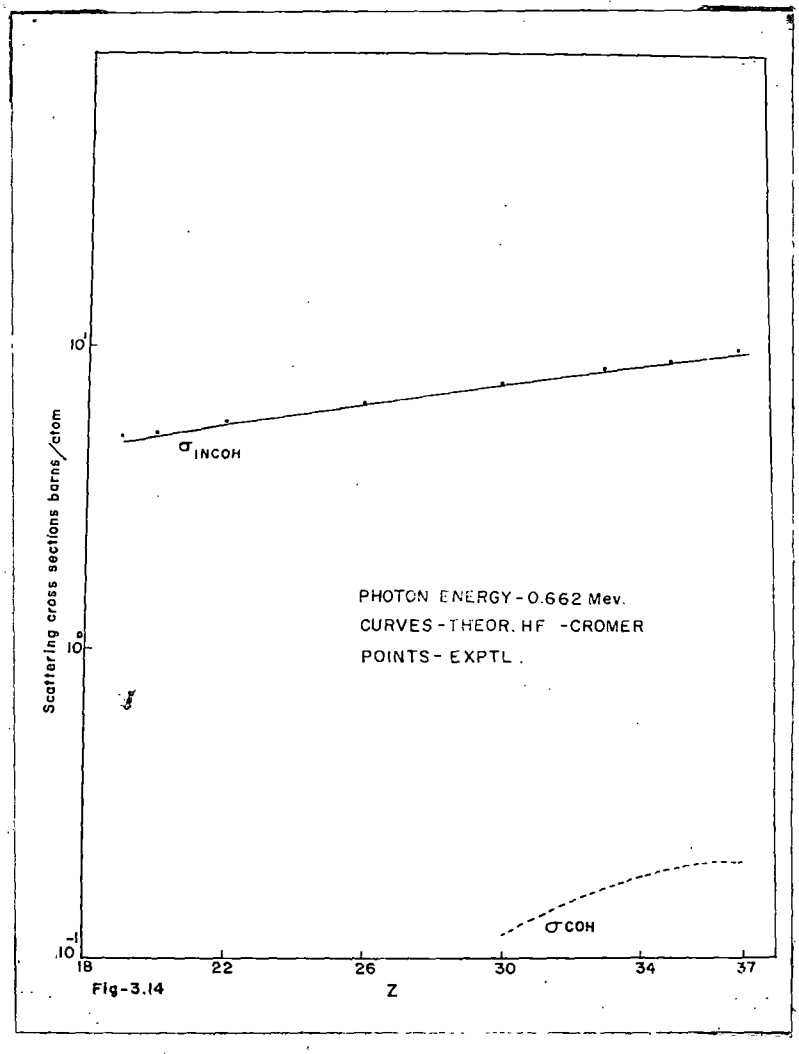
Scattering cross sections barns/atom
10^1
10^0
10^{-1}
σ_{INCOH}
PHOTON ENERGY - 0.662 Mev.
CURVES - THEOR. HF - CROMER
POINTS - EXPTL.
σ_{COH}
18
22
26
30
34
37
Z

Fig-3.14

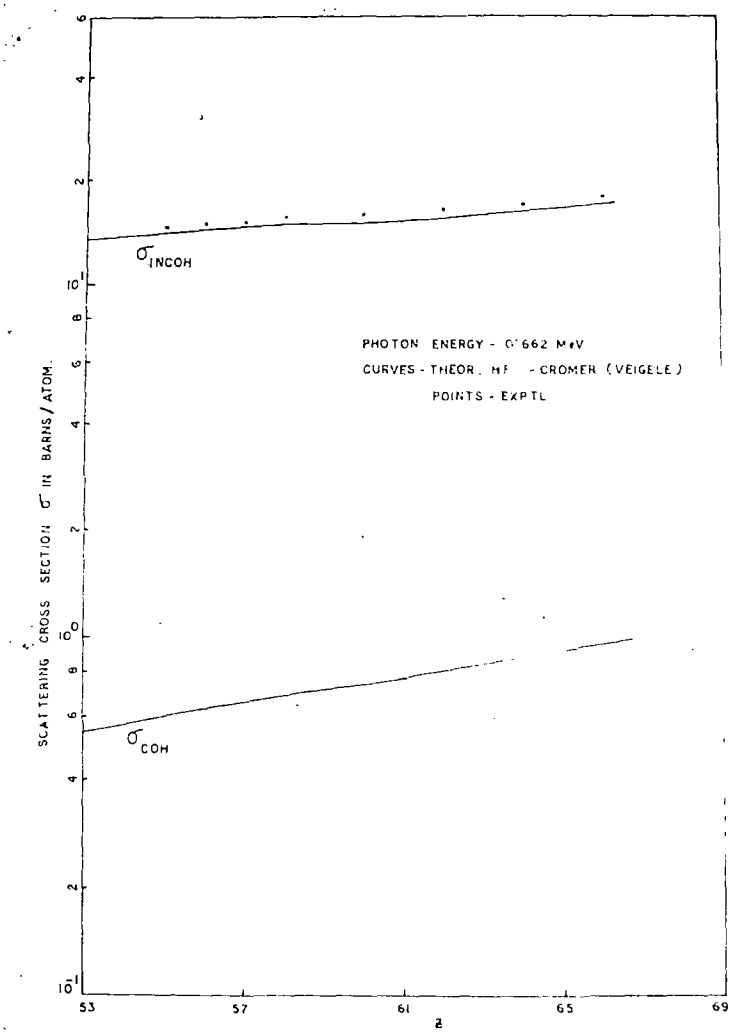
SCATTERING CROSS SECTION σ IN BARNS/ATOM.
σ INCOH
σ COH
PHOTON ENERGY - 0·662 MeV
CURVES - THEOR. HF - CROMER (VEIGELE)
POINTS - EXPTL
Z
53
57
61
65
69

FIG. 3·15.

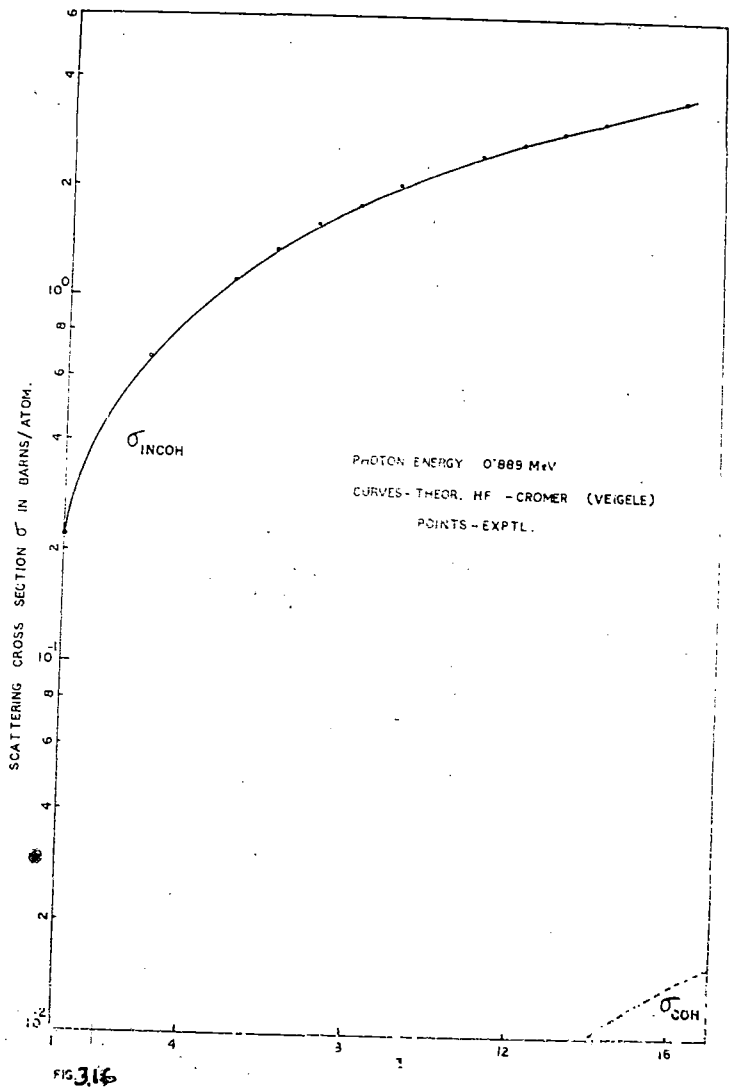
SCATTERING CROSS SECTION σ IN BARNS/ATOM.
σ INCOH
PHOTON ENERGY 0·889 MeV
CURVES - THEOR. HF - CROMER (VEIGELE)
POINTS - EXPTL.
σ COH
1
4
3
12
16

FIG 3.16

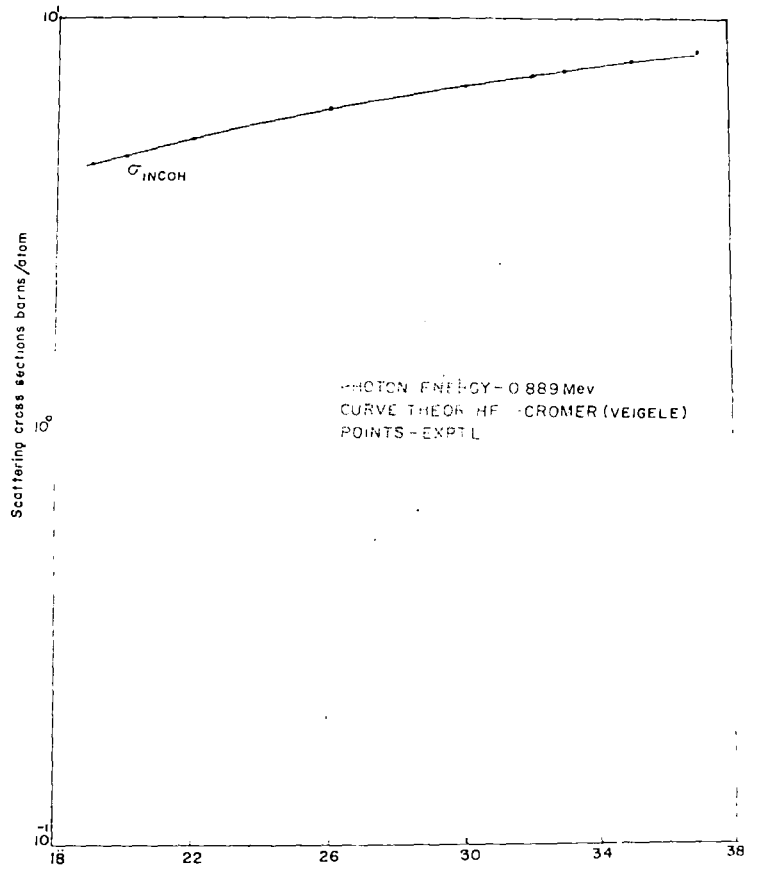
Scattering cross sections barns/atom
10^1
10^0
10^{-1}
σ_{INCOH}
PHOTON ENERGY - 0.889 Mev
CURVE THEOR HF CROMER (VEIGELE)
POINTS - EXPTL
18
22
26
30
34
38
Z

Fig. 3.17

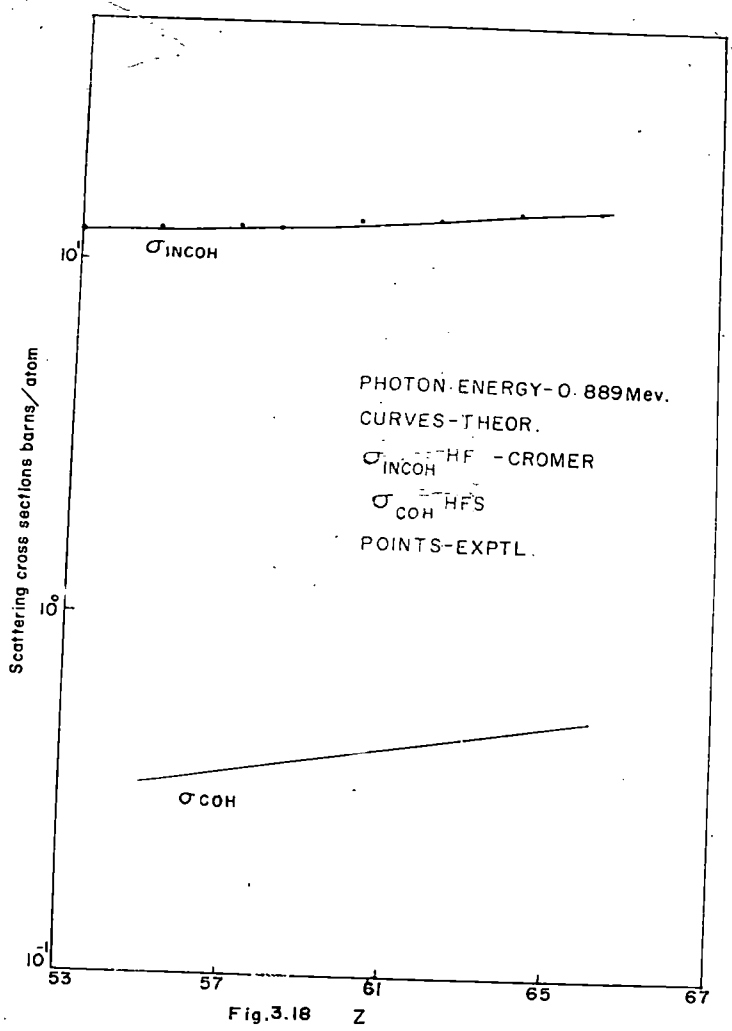
Scattering cross sections barns/atom
10^1
10^0
10^{-1}
σ_{INCOH}
σ_{COH}
PHOTON ENERGY- 0.889 Mev.
CURVES-THEOR.
σ_{INCOH} HF -CROMER
σ_{COH} HFS
POINTS-EXPTL.
53
57
61
65
67
Z

Fig.3.18

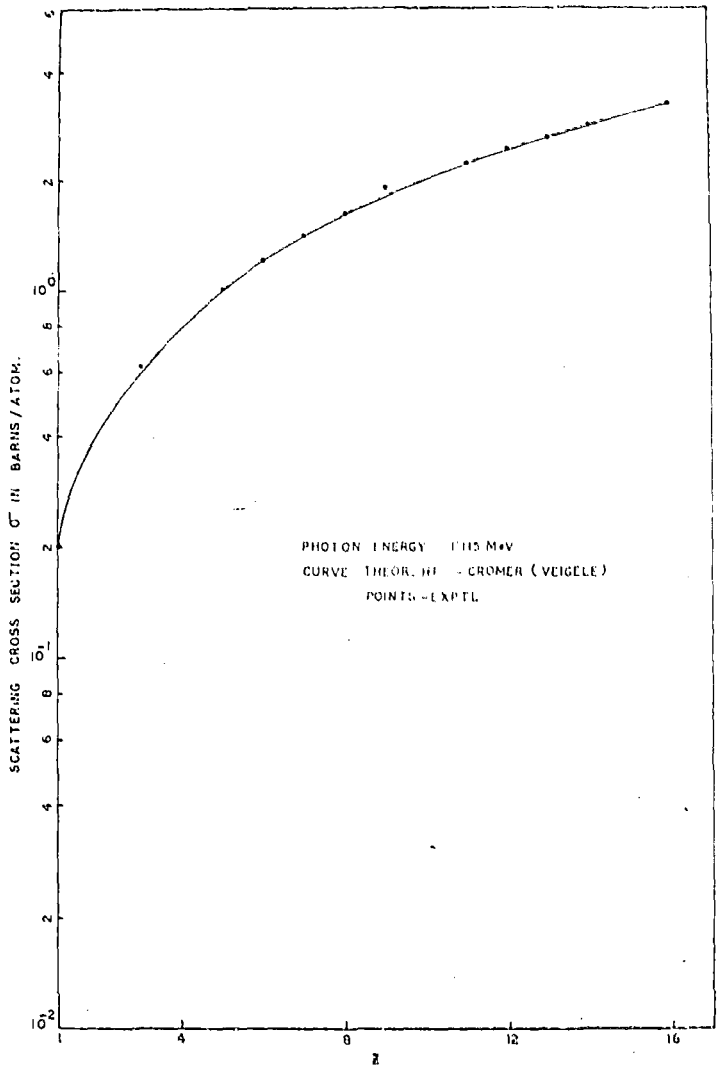
SCATTERING CROSS SECTION σ IN BARNS / ATOM.
PHOTON ENERGY 1.115 MeV
CURVE THEOR. HE - CROMER (VEIGELE)
POINTS - EXPTL.
Z

FIG. 3'19.

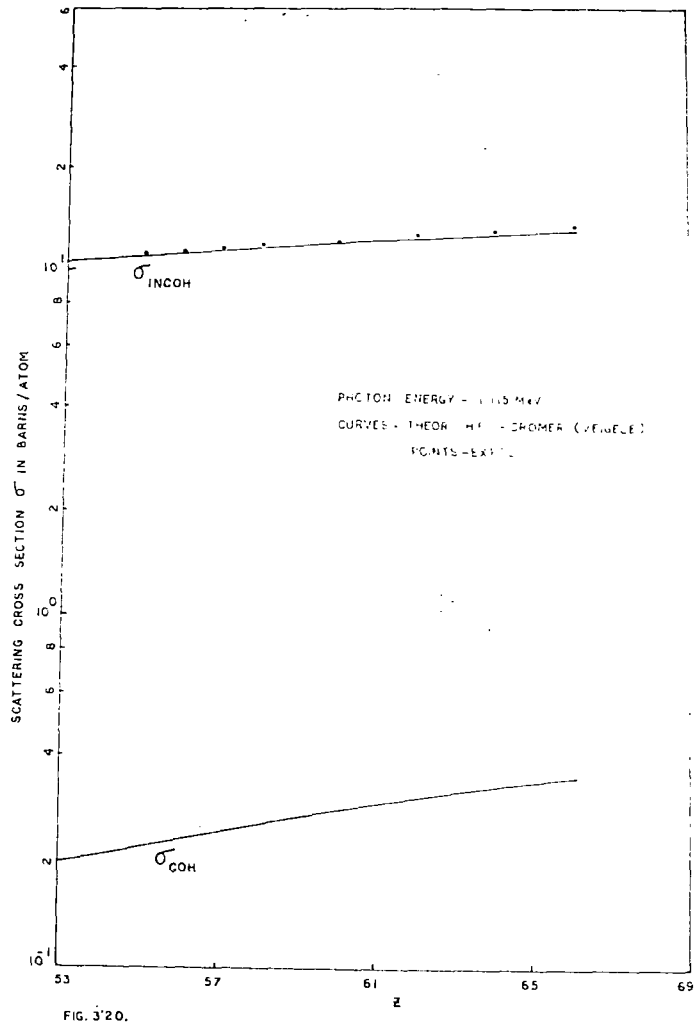
SCATTERING CROSS SECTION σ IN BARNS/ATOM
σ INCOH
σ COH
PHOTON ENERGY
CURVES
POINTS
Z
53
57
61
65
69

FIG. 3'20.

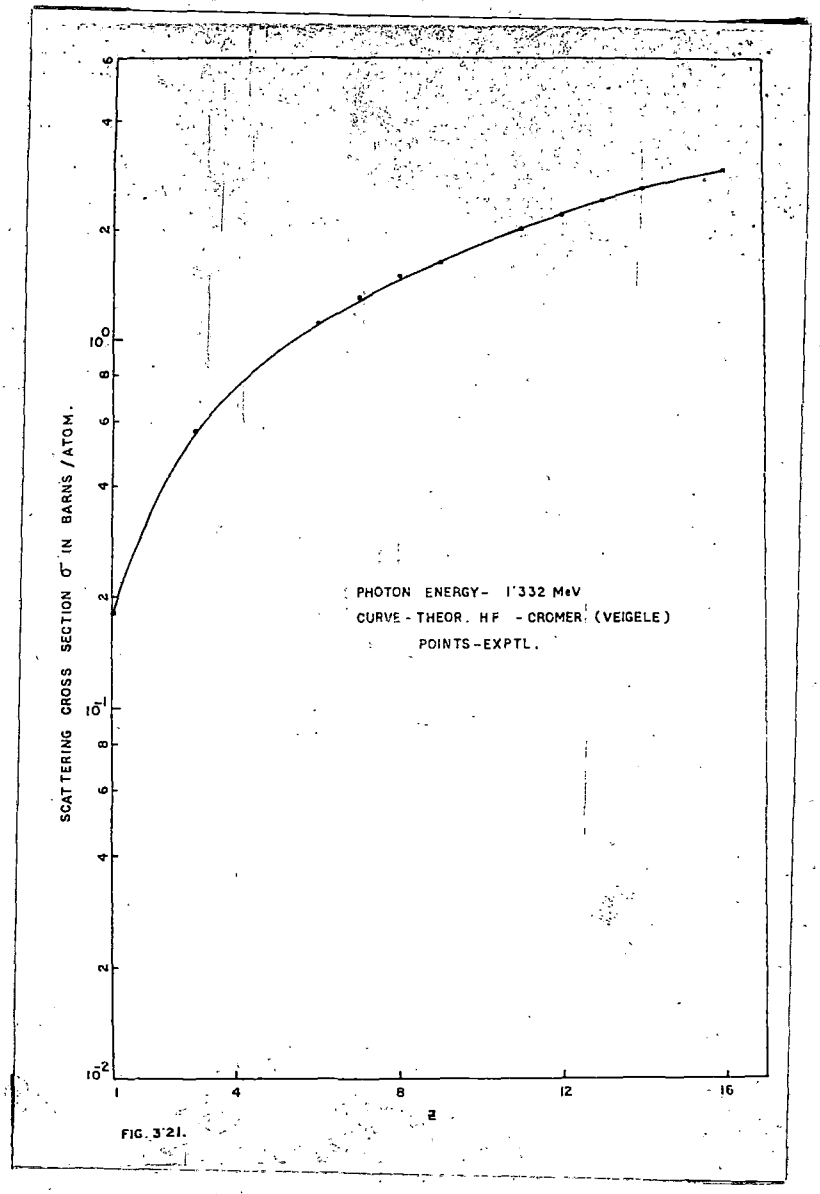
SCATTERING CROSS SECTION σ IN BARNS / ATOM.
PHOTON ENERGY- 1·332 MeV
CURVE - THEOR. HF - CROMER (VEIGELE)
POINTS - EXPTL.
Z

FIG. 3·21.

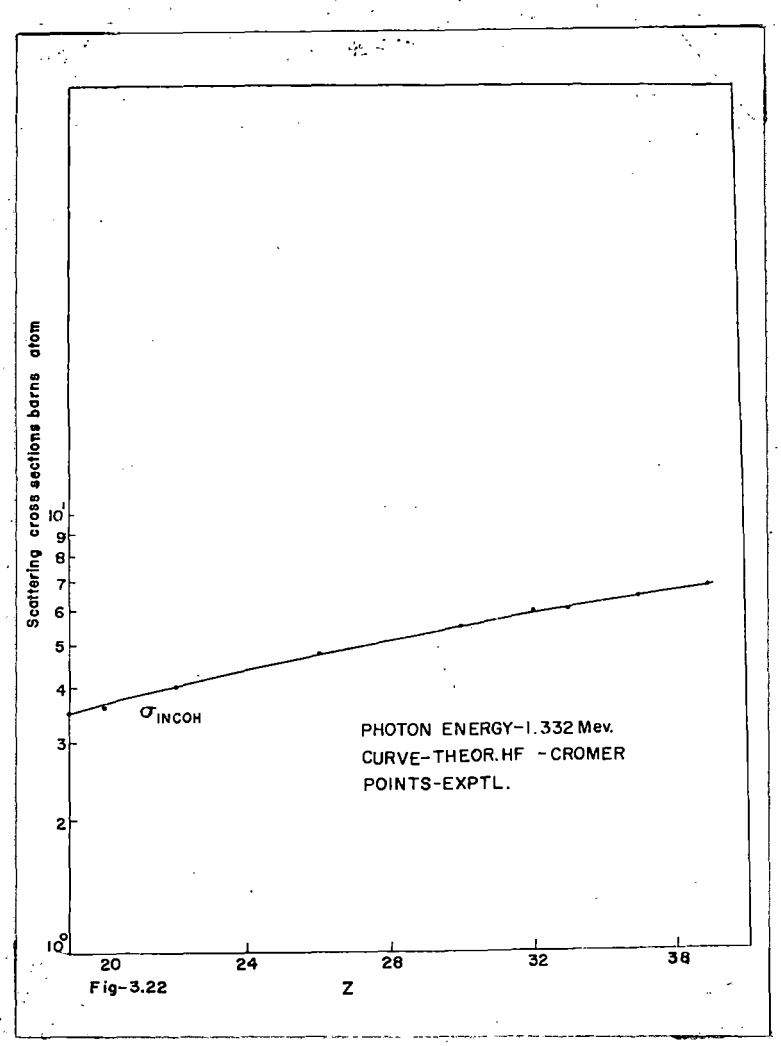
Scattering cross sections barns atom
10
9
8
7
6
5
4
3
2
10°
20
24
28
32
38
Z
σ INCOH
PHOTON ENERGY-1.332 Mev.
CURVE-THEOR.HF -CROMER
POINTS-EXPTL.

Fig-3.22

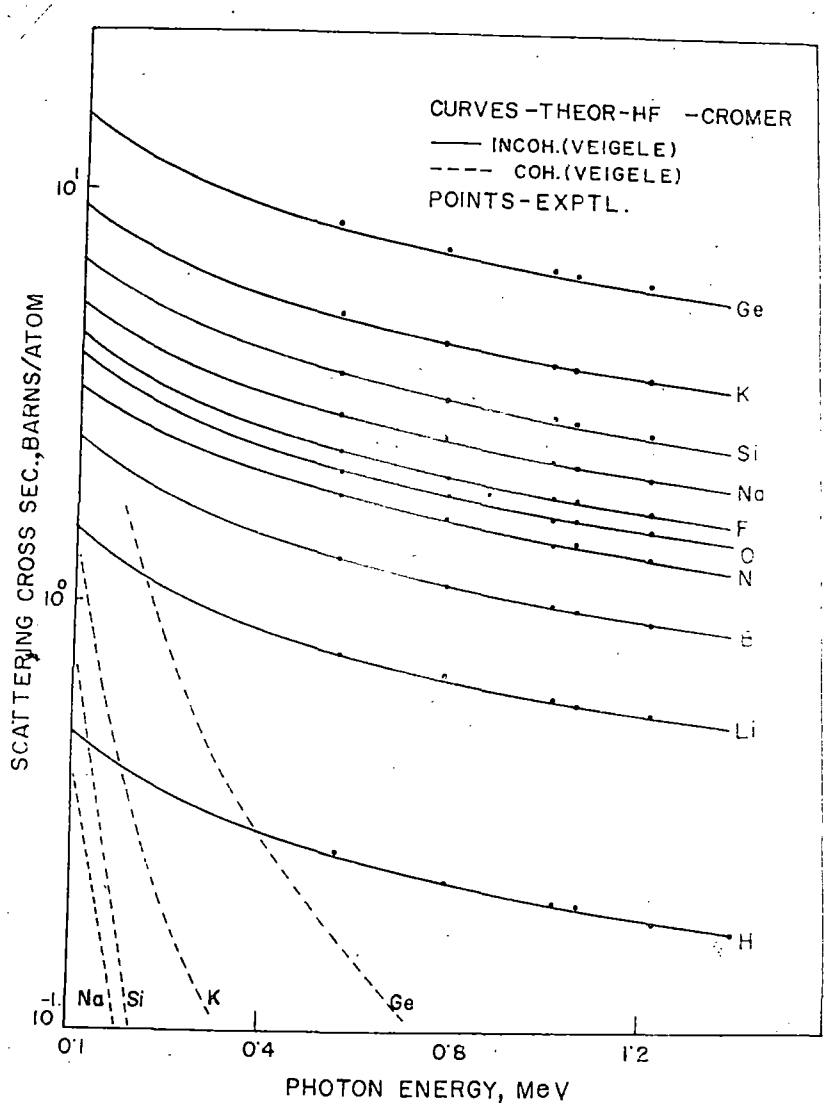
CURVES-THEOR-HF -CROMER
INCOH.(VEIGELE)
COH.(VEIGELE)
POINTS-EXPTL.
Ge
K
Si
Na
F
O
N
B
Li
H
Na
Si
K
Ge
10^1
10^0
10^{-1}
0·1
0·4
0·8
1·2
SCATTERING CROSS SEC., BARNS/ATOM
PHOTON ENERGY, MeV

Fig. 3.8

3.5.2. Discussion and Interpretation of the experimental total scattering data.

In interpreting the experimental scattering cross sections we consider only the scattering processes which are dominant in the energy region of the present work. These are the incoherent scattering and atomic Rayleigh scattering. The coherent contributions of nuclear Thomson scattering and Delbrück scattering in the energy range below and near 1 MeV will be negligible. Theoretically, the average total incoherent and atomic Rayleigh scattering cross sections can be calculated by equations 1.17 and 1.23 using Cromer's values of incoherent scattering function S and form factor F. This computation has been done by Storm and Israel (St 70) using Cromer's S values and F values of Hansen et al (Ha 64). Recently Veigele et al (V 71) computed these total cross sections using Cromer's S and F values for elements from Z = 1 to Z = 94. We have used these computed data to interpret the present experimental total scattering cross sections in the following way.

The calculated total cross sections σ_{INCOH} and σ_{COH} and $(\sigma_{INCOH} + \sigma_{COH})$ for various elements studied are presented in graphs along with the present results. These graphs for the whole energy range from 662 KeV to 1332 KeV compare our experimental data with the corresponding theoretical values.

A. Photon energy vs. cross section graphs.

As already pointed out, in the energy range of the present work, the incoherent scattering process dominates over almost the whole range of Z investigated. The graphs in figs. 3.8 - 3.12 represent the data only for some representative elements selected on the basis of the following consideration. According to the extensive survey of Hubbell (Hu 71) hydrogen(Z=1)

although its scattering cross sections has been calculated exactly has not been measured in the present energy range. Lithium (Z=3) boron (Z=5) nitrogen (Z=7) oxygen (Z=8) fluorine (Z=9) have no previous data in the same energy range. Sodium has only one measurement in the present energy range. For silicon (Z=14) there are three previous data points (Ma 70), x (Bo 58) in the energy range 1.12 to 1.33 MeV. Potassium (Z=19) again has no experimental data in this energy range. Except for one G.M. counter data at 1.25 MeV for germanium (Z=32), (Bo 58), we have not found in Hubbell's survey any other reference to cross section measurements in the energy range considered. Rubidium (Z =37) has also no publishsed data. In the range of higher Z elements cesium (Z=55) has no published data. In the rare earth group, cesium (Z =58). Neodymium (Z=60), samarium (Z=62), dysprosium(Z=66) and Ytterbium (Z=70) which have no previous data in this energy range have been measured in the present work. In these graphs, it can be seen that our data are in best fit with the computed theoretical curves. Our germanium data also appear to match well with the total cross sections $\sigma_{INCOH} + \sigma_{COH}$. The previous silicon data mentioned above (Ma 70, Bo 58) did not fit with the theory well.

B. Z vs. cross section graphs.

Our data set for all the elements investigated are also presented to show variation of cross section with atomic number Z at each energy in the present energy range figs. 3.13 to 3.22. Except for the experimental point at 1.115 MeV for fluorine (Z=9) our experimental Z vs. cross section plots are in good agreement with the theoretically predicted cross sections considering incoherent scattering process and coherent Rayleigh scattering process for elements where it becomes contributing to the total cross section. The experimental data at 1.332 MeV for higher Z elements investigated are given in table 3.12 where theoretical values of σ_{INCOH}, and σ_{COH} & σ_{TOT} are also included

for comparison with the measured data. As can be seen in this table, the theoretical σ_{TOT} values are in fair agreement with the present data at this energy with a maximum of 3 percent deviation in case of lead.

TABLE 3.12

Comparison of experimental and theoretical scattering cross sections. (The uncertainty in the last decimal place is shown in the parentheses).

Photon energy 1.332 MeV.

Element	Z	Experimental (barns/atom)	Theoretical (barns/atom) σ_{INCOH} (HF-CROMER)	σ_{COH} (HFS-SPONM-ISRAEL)	σ_{Tot}
Mo	42	7.76(5)	7.70	0.075	7.75
I	53	9.94(2)	9.67	0.14	9.81
Cs	55	10.24(4)	10.08	0.15	10.23
Ba	56	10.43(5)	10.26	0.16	10.42
La	57	10.60(7)	10.45	0.17	10.62
Ce	58	10.78(7)	10.65	0.18	10.83
Nd	60	11.48(7)	11.23	0.19	11.42
Sm	62	11.53(8)	11.31	0.21	11.52
Gd	64	11.98(8)	11.78	0.23	12.01
Dy	66	12.38(8)	12.12	0.25	12.37
Yb	70	13.25(9)	12.81	0.29	13.10
Hg	80	14.92(3)	14.55	0.40	14.95
Pb	82	15.37(3)	14.96	0.43	15.39

Discussing the earlier experimental data in this energy range we chose only the most recent measurement by Conner et al. In table 3.13 a comparison of data is given for some elements which are common among their measurement and the present measurement. The agreement of the two sets of data is seen to be excellent.

TABLE 3.13

Comparison of total scattering cross section with those obtained from the measurement of Conner et al(Co 70) for some common elements at 0.662 MeV and 1.115 MeV(barns/atom)

Element Z	Energy(MeV)	Present measurements	Conner et al.
6	0.662	1.54(1)	1.538(7)
	1.115	1.20(0)	
12	0.662	3.08(3)	3.088(18)
	1.115	2.41(1)	
13	0.662	3.33(3)	3.327(11)
	1.115	2.61(1)	
16	0.662	4.15(3)	4.147(22)
	1.115	3.21(1)	
22	0.662	5.66(10)	5.651(18)
	1.115	4.41(2)	4.433(23)

TABLE 3.13(Contd.)

Element Z	Energy (MeV)	Present measurements	Conner et al.
26	0.662	6.70(4)	6.647(20)
	1.115	5.23(1)	5.172(17)
30	0.662	7.77(1)	7.763(33)
	1.115	6.04(1)	6.032(23)
42	0.662	11.0(2)	10.897(38)
	1.115	8.51(5)	8.466(27)
57	0.662	15.2(3)	15.06(5)
	1.115	11.5(1)	11.49(6)
64	0.662	17.3(4)	16.79(8)
	1.115	13.1(1)	13.04(7)
82	0.662	22.0(3)	22.03(17)
	1.115	17.04(3)	16.77(11)

(In parentheses is given the uncertainty in the last one or two places)

The present set of measurements according to our information, provide the most comprehensive and accurate experimental scattering cross section data in the energy range under consideration.

3.5.3. Conclusions.

Our experimental data and their analysis given above show that

(i) when several systematic errors in the transmission measurement are eliminated the attenuation experiments using photons near 1.0MeV in low, intermediate and high Z elements (upto Z =82) yield very accurate total cross sections;

(ii) the presently available accurate theoretical knowledge of atomic photoabsorption and pair production cross sections, which permit their being subtracted from the measured total cross sections lead to accurate total scattering cross sections;

(iii) the experimental total scattering data thus obtained are in excellent fit (except in one or two cases) with the integral cross section σ_{INCOH} for incoherent scattering evaluated on the SCF HF model (after Cromer) for elements where coherent scattering processes are not dominating. For higher Z elements our data are in satisfactory match with the sum of the integral σ_{INCOH} and integral σ_{COH} evaluated on the HF model (after Cromer).

Finally, it may be stated that the present data provide a satisfactory verification of Cromer's theory of coherent and incoherent scattering of photons in the energy range considered.